# Rapid and robust optogenetic control of gene expression in Drosophila

Florencia Di Pietro, Sophie Herszterg, Anqi Huang, Floris Bosveld, Cyrille Alexandre, Lucas Sancéré, Stéphane Pelletier, Amina Joudat, Varun Kapoor, Jean-Paul Vincent, et al.

Technology

Developmental Cell

# Rapid and robust optogenetic control of gene expression in *Drosophila*

## Graphical abstract

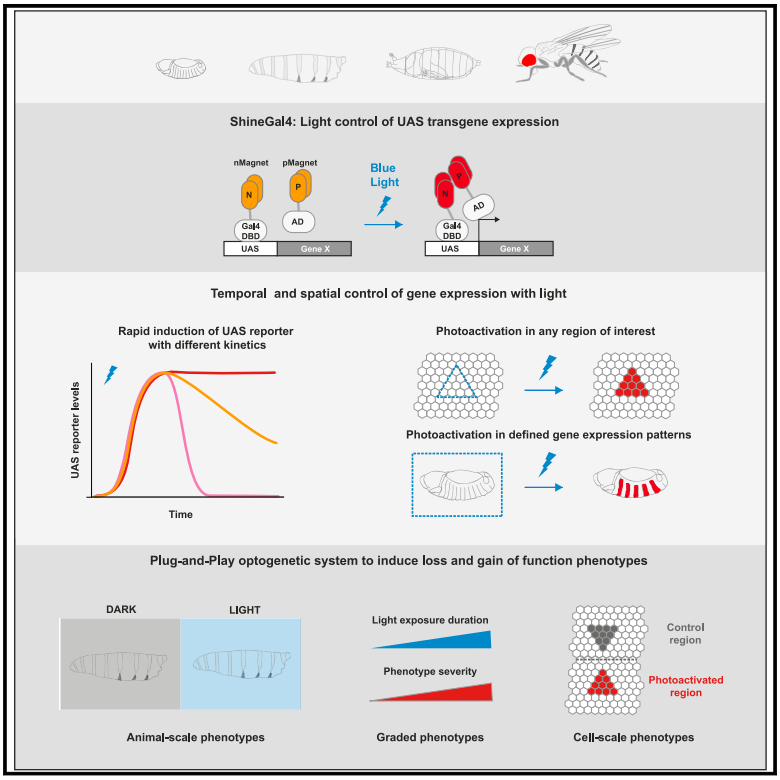


## Highlights

- ShineGal4 is a *Drosophila* transgenic optogenetic Gal4 system
- It allows rapid and robust light activation of UAS reporters in various tissues
- It can be actuated in given regions of interest or enhancer-defined patterns
- ShineGal4 enables the exploration of gene function with high spatiotemporal resolution

## Authors

Florencia di Pietro, Sophie Herszterg, Anqi Huang, ..., Varun Kapoor, Jean-Paul Vincent, Yohanns Bellaïche

## Correspondence

jp.vincent@crick.ac.uk (J.-P.V.), yohanns.bellaiche@curie.fr (Y.B.)

## In brief

di Pietro et al. develop a GAL4/UAS optogenetic system that allows fast and efficient control of gene expression. This enables the investigation of gene function with high spatiotemporal resolution in *Drosophila in vivo*.

di Pietro et al., 2021, Developmental Cell *56*, 1–12
December 20, 2021 
https://doi.org/10.1016/j.devcel.2021.11.016

CellPress

Developmental Cell

CellPress
OPEN ACCESS

Technology

# Rapid and robust optogenetic control of gene expression in *Drosophila*

Florencia di Pietro,[1] Sophie Herszterg,[2] Anqi Huang,[2] Floris Bosveld,[1] Cyrille Alexandre,[2] Lucas Sancéré,[1] Stéphane Pelletier,[1] Amina Joudat,[1] Varun Kapoor,[1] Jean-Paul Vincent,[2,*] and Yohanns Bellaïche[1,3,*]

[1]Institut Curie, Université PSL, Sorbonne Université, CNRS UMR 3215, Inserm U934, Genetics and Developmental Biology, 75005 Paris, France

[2]Francis Crick Institute, 1 Midland Rd, London NW1 1AT, UK

[3]Lead contact

*Correspondence: jp.vincent@crick.ac.uk (J.-P.V.), yohanns.bellaiche@curie.fr (Y.B.)

https://doi.org/10.1016/j.devcel.2021.11.016

## SUMMARY

Deciphering gene function requires the ability to control gene expression in space and time. Binary systems such as the Gal4/UAS provide a powerful means to modulate gene expression and to induce loss or gain of function. This is best exemplified in *Drosophila*, where the Gal4/UAS system has been critical to discover conserved mechanisms in development, physiology, neurobiology, and metabolism, to cite a few. Here we describe a transgenic light-inducible Gal4/UAS system (ShineGal4/UAS) based on Magnet photoswitches. We show that it allows efficient, rapid, and robust activation of UAS-driven transgenes in different tissues and at various developmental stages in *Drosophila*. Furthermore, we illustrate how ShineGal4 enables the generation of gain and loss-of-function phenotypes at animal, organ, and cellular levels. Thanks to the large repertoire of UAS-driven transgenes, ShineGal4 enriches the *Drosophila* genetic toolkit by allowing *in vivo* control of gene expression with high temporal and spatial resolutions.

## INTRODUCTION

Experimental control of gene expression in space and time is instrumental in deciphering the basic principles governing metazoan development, homeostasis, and physiology. Over the last 25 years, the binary Gal4/UAS expression system, initially introduced in *Drosophila* (Brand and Perrimon, 1993), has become an essential tool to control gene expression in numerous animal systems (Adolfi et al., 2018; Caygill and Brand, 2016; Kawakami et al., 2016; Del Valle Rodríguez et al., 2011). This stems from the combinatorial possibilities offered by the pairwise use of UAS-driven transgenes and Gal4-expressing transgenes controlled by specific promoters, allowing loss- and gain-of-function studies in given tissues or cells, as well as lineage tracing of specific cell types. Accordingly, the shared resources of transgenic Gal4 drivers and UAS transgenes endow researchers with ever-increasing collections of tools to explore patterning, signaling, neurogenesis, and physiology, to name a few (Caygill and Brand, 2016; Dietzl et al., 2007; Jenett et al., 2012; Kaya-Çopur and Schnorrer, 2016; Kvon et al., 2014; Port et al., 2020; Zirin et al., 2020).

The success of the Gal4/UAS system has, furthermore, led to additional refinements to better control UAS-driven transgene expression, in space with split-Gal4 drivers (Pfeiffer et al., 2010) or in time by exploiting hormone-dependent transactivation domains (Nicholson et al., 2008; Wang et al., 1997) or the temperature-sensitive Gal80 ($Gal80^{ts}$) repressor (McGuire et al., 2003; Zeidler et al., 2004). However, these approaches rely on the availability of promoters controlling Gal4 expression only at specific developmental stages. They are also subject to the slow $Gal80^{ts}$ kinetics as well as the confounding effects of temperature changes or hormonal supplementation (Landis et al., 2015; McGuire et al., 2003; Zeidler et al., 2004). Optogenetics promises to overcome these limitations by readily providing control of gene expression both in space and time (de Mena et al., 2018). Accordingly, there have been several attempts to develop optogenetic binary systems (de Mena et al., 2018). Some success has been reported with optogenetic Gal4 approaches in cell culture, zebrafish embryos, *Drosophila*, and mice (Liu et al., 2012; Wang et al., 2012; Pathak et al., 2017; de Mena and Rincon-Limas, 2020; Mruk et al., 2020; Yamada et al., 2020). These advances are significant, but they come with some limitations: (i) the long light exposure (in the order of hours) necessary to induce phenotypes or reporter expression (de Mena and Rincon-Limas, 2020; Mruk et al., 2020), likely incompatible with live imaging or the study of rapid biological processes; (ii) leakiness in the dark (Mruk et al., 2020; Pathak et al., 2017; Yamada et al., 2020); (iii) the lack of a fully transgenic optogenetic Gal4/UAS system (Liu et al., 2012; Pathak et al., 2017; Yamada et al., 2020); or (iv) the requirement of an exogenous chromophore, which is only readily administered to tissue explants (de Mena and Rincon-Limas, 2020). Accordingly, the use of optogenetic Gal4/UAS systems continues to be sparse. More generally, there is no current optogenetic binary system

Please cite this article in press as: di Pietro et al., Rapid and robust optogenetic control of gene expression in *Drosophila*, Developmental Cell (2021), https://doi.org/10.1016/j.devcel.2021.11.016



that leverages the combinatorial possibilities afforded by existing shared resources.

Here, we report the development of a light-inducible split-Gal4 that provides rapid and robust gene expression control in space and time in *Drosophila in vivo*. We establish that this light-inducible Gal4, which we call ShineGal4, can be used to induce gain- and loss-of-function phenotypes with high temporal and spatial resolution. We expect that the ShineGal4/UAS system will open new experimental opportunities to decipher a broad range of biological processes.

## Design

A set of exploratory experiments indicated that the LOV (Wang et al., 2012), Cry2/CIBN (Kennedy et al., 2010), and iLID/SspB (Guntas et al., 2015) optogenetic modules were unlikely to be suitable for an efficient Gal4-based transgenic optogenetic system. We therefore turned to Magnet (Mag) photoswitches (Kawano et al., 2015), which comprise negatively charged nMag and positively charged pMag proteins that heterodimerize in response to blue light (Figure 1A). Several nMag and pMag variants have been developed to achieve different efficiencies of light-dependent heterodimerization and switch-off kinetics by introducing point mutations in photocycle-related residues (Kawano et al., 2015). As a first step, we opted for the MagHigh1 variants, which exhibit the highest interaction strength under light with a half-life ($t_{1/2}$) switch-off kinetics of 4.7 h (Kawano et al., 2015). Because higher interaction strengths are achieved by multimerizing Magnet photoswitches (Kawano et al., 2015), two tandem repeats of nMagHigh1 and pMagHigh1 were fused to the Gal4 DNA binding domain (1–147 aa, Gal4DBD; Carey et al., 1989) and the p65 transactivation domain (425–548 aa, AD; Pfeiffer et al., 2010), respectively, to generate the Gal4DBD:2xnMagHigh1 and 2xpMagHigh1:AD fusion genes (Figure 1A).

Gal4DBD:2xnMagHigh1 and 2xpMagHigh1:AD could be expressed as a single transcript using a T2A sequence to promote a self-cleavage into the Gal4DBD:2xnMagHigh1 and 2xpMagHigh1:AD proteins during translation (Lo et al., 2015). However, because this design might lead to background activity from the small amount of fusion protein arising from incomplete T2A cleavage, we opted to express Gal4DBD:2xnMagHigh1 and 2xpMagHigh1:AD from two separate transgenes under the control of the ubiquitin (ubi) promoter and with a p10 3′ UTR to improve mRNA stability and boost expression (Pfeiffer et al., 2012) (Figure 1B). In preliminary experiments, this led to reporter expression under light. We thus pursued to characterize the ubi-Gal4DBD:2xnMagHigh1-p10 and ubi-2xpMagHigh1:AD-p10 combination of transgenes, which we refer to as ubi-Gal4$^{MagHigh}$. In some circumstances, it might be beneficial that light-induced expression terminates rapidly after the light is turned off. We, therefore, created constructs with Magnet variants that have faster switch-off kinetics. For instance, in combination with nMagHigh1, the pMag, pFast1, and pFast2 variants have a $t_{1/2}$ switch-off kinetics of 1.8 h, 4.2 min, and 25 s, respectively, compared with the 4.7 h switch-off kinetics of the nMagHigh1-pMagHigh1 combination (Kawano et al., 2015). We built ubi-2xpMag:AD-p10, ubi-2xpMagFast1:AD-p10, and ubi-2xpMagFast2:AD-p10 transgenes with the aim of testing them in combination with ubi-Gal4DBD:2xnMagHigh1-p10. We refer to these transgene combinations as ubi-Gal4$^{Mag}$, ubi-Gal4$^{MagFast1}$, and ubi-Gal4$^{MagFast2}$.

## RESULTS

### Temporal control of gene expression

As a first step, we quantitatively analyzed the ability of ubi-Gal4$^{MagHigh}$ to drive UAS reporter expression in response to blue light in the *Drosophila* pupal dorsal thorax epithelium (notum, Figure 1C), a model to study cell and tissue dynamics by live imaging (Bosveld et al., 2012, 2016; Curran et al., 2017; Founounou et al., 2013; Guirao et al., 2015; Herszterg et al., 2013; Levayer et al., 2016; López-Gay et al., 2020; Pinheiro et al., 2017). For this, ubi-Gal4$^{MagHigh}$, UAS-His2B:RFP (ubi-Gal4$^{MagHigh}$>His2B:RFP) animals expressing the adherens junction (AJ) marker Ecad:GFP were raised in the dark. At the pupal stage, they were mounted under amber light for spinning disc confocal live microscopy (see STAR Methods). The level of His2B:RFP in these pupae was similar to that observed in pupae carrying only the UAS-His2B:RFP reporter, indicating minimal dark background activity (Figure S1A). We then illuminated a 20-section z stack (200 ms per z position) every 5 min at 491 nm (0.5 mW) to induce Mag heterodimerization as well as to image the Ecad:GFP signal. At the same time, 561-nm illumination was used to record His2B:RFP levels (See Table S1A for detailed illumination and acquisition conditions). The His2B:RFP signal became detectable in the whole tissue as early as 2 h after the onset of 491-nm illumination (Figure 1D; Video S1). The His2B:RFP signal was initially variable among cells, but later became homogeneous and reached a maximal 35 ± 6-fold average induction (Figures 1D and 1E; Video S1). As expected, the use of amber light illumination during staging and mounting was critical to avoid photoactivation prior to imaging, and exposure to 561-nm illumination did not promote His2B:RFP expression in ubi-Gal4$^{MagHigh}$>His2B:RFP pupae (Figures S1B and S1C). The ability of the ubi-Gal4$^{MagHigh}$ driver to control gene expression upon blue light illumination was further confirmed using different reporters, including UAS-His2B:YFP and UAS-LifeAct:GFP (Figures S1D and S1E). Importantly, in all cases, the 491-nm photoactivation settings used to induce reporter expression were fully compatible with the illumination conditions used for live imaging of cell and tissue dynamics with minimal phototoxicity.

Having found that ubi-Gal4$^{MagHigh}$ photoactivation induces gene expression, we further characterized its switch-on kinetics using the UAS-His2B:RFP reporter. As shown in Figure 1G, the ubi-Gal4$^{MagHigh}$ switch-on $t_{1/2}$ is 4.9 ± 0.1 h, with His2B:RFP reaching maximal levels within 8 h. To investigate how this delay compares to the time required for His2B:RFP synthesis, maturation, and exchange with untagged histones, we performed FRAP experiments in pupae expressing UAS-His2B:RFP under the control of the ubiquitous actin-Gal4 driver (act-Gal4). Upon photobleaching, the His2B:RFP signal recovered with a $t_{1/2}$ of 4.6 ± 0.1 h, which is similar to that observed with ubi-Gal4$^{MagHigh}$ (Figures 1G and S1F). This indicates that His2B:RFP synthesis, maturation, or exchange are limiting factors for the accumulation of newly synthesized His2B:RFP upon photoactivation. By comparison, the accumulation of His2B:RFP with act-Gal4/tub-Gal80$^{ts}$ became only detectable 7 h after a temperature shift from 18°C to 29°C ($t_{1/2}$ equals 10.9 ± 0.6 h, Figures 1F and 1G). Furthermore, the maximal His2B:RFP level obtained using

Please cite this article in press as: di Pietro et al., Rapid and robust optogenetic control of gene expression in *Drosophila*, Developmental Cell (2021), https://doi.org/10.1016/j.devcel.2021.11.016



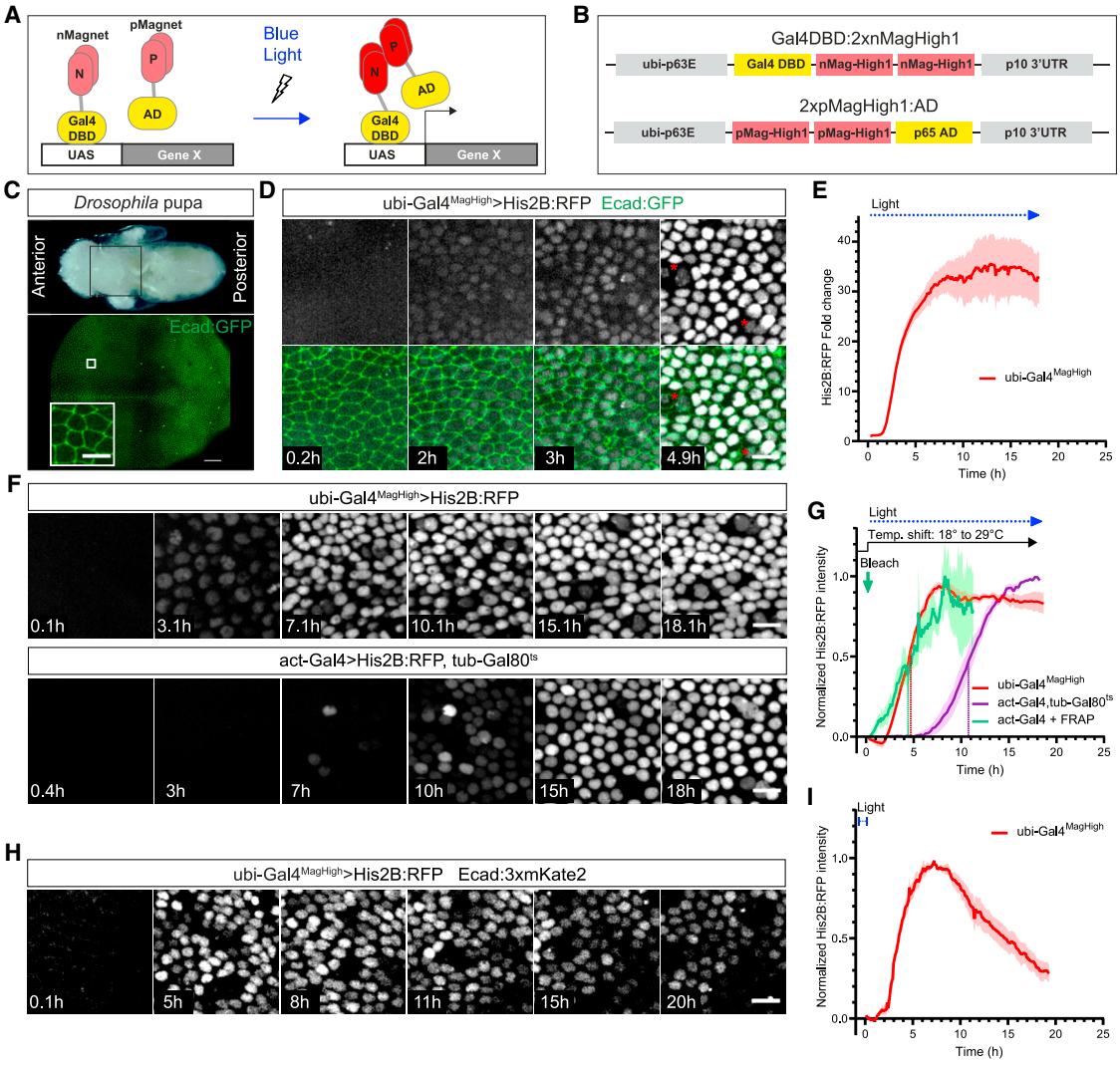


**Figure 1. Temporal control of gene expression in the pupal dorsal thorax (notum)**

Illumination settings used for photoactivation and imaging are given in Table S1A. N, number of animals.

(A) Schematic representation of the optogenetic split Gal4-Magnets used to induce gene expression by blue light photoactivation. Gal4 DBD (aa 1–147) and p65 AD (aa 425–548) are respectively fused to nMagnet and pMagnet tandems, which heterodimerize upon blue light exposure and promote Gal4-mediated activation of gene expression.

(B) Transgenes used to ubiquitously express Gal4DBD:2xnMagHigh1 and 2xpMagHigh1:AD.

(C) Dorsal view of a 14 h after pupa formation (hAPF) *Drosophila* pupa (top, from Bosveld et al., 2012) and a multiposition confocal image of the notum epithelium (bottom), showing the distribution of Ecad:GFP. The black box indicates the region shown in the bottom panel. Inset: close-up on Ecad:GFP distribution in the region outlined by a white box.

(D) Time-lapse images of ubi-Gal4$^{MagHigh}$>His2B:RFP (top and bottom) and Ecad:GFP (bottom) upon photoactivation. Time (h) is set to 0 at the start of the 491-nm illumination. Red asterisks indicate sensory organ precursors, the nuclei of which are located more basally.

(E) Graph of His2B:RFP fold change (mean ± SEM, N = 5) during photoactivation. Time (h) is set to 0 at the start of the 491-nm illumination.

(F) Time-lapse images of ubi-Gal4$^{MagHigh}$>His2B:RFP (top) and act-Gal4>His2B:RFP, tub-Gal80$^{ts}$ (bottom). Time (h) is set to 0 at the start of the 491-nm illumination or upon temperature shift from 18°C to 29°C.

(G) Graph of the normalized His2B:RFP intensity (mean ± SEM) for the experiments shown in (F) (red, N = 5 and purple, N = 3) and upon His2B:RFP photobleaching (FRAP) in act-Gal4>His2B:RFP pupae (green, N = 4). Red and purple curves: values are normalized to the maximal ones in each condition. Green curve: values of the bleached region are normalized to the ones of the non-bleached region. Dashed lines: $t_{1/2}$ of His2B:RFP protein accumulation. See also Figures S1F and S1G.

(H) Time-lapse images of ubi-Gal4$^{MagHigh}$>His2B:RFP following a 1 h pulsed 491-nm illumination. Images are taken in the plane of the nucleus, the AJ Ecad:3xmKate2 is not visible. Time (h) is set to 0 at the end of the 491-nm illumination.

(I) Graph of normalized His2B:RFP intensity (mean ± SEM, N = 4) for the experiment shown in (H). To ensure that His2B:RFP is accurately quantified, the measured His2B: RFP intensity is corrected by the background intensity due to Ecad:3xmKate2 signal in the nuclei plane. Values are normalized to the maximal value.

Scale bars: 50 μm (C) and 10 μm (D, F, H, and inset in C).

See also Figures S1 and S2 as well as Video S1; Table S1A.

Please cite this article in press as: di Pietro et al., Rapid and robust optogenetic control of gene expression in *Drosophila*, Developmental Cell (2021), https://doi.org/10.1016/j.devcel.2021.11.016



ubi-Gal4$^{MagHigh}$ was only slightly lower than the one achieved using act-Gal4/tub-Gal80$^{ts}$ (Figure S1G). Using the His2B:RFP reporter, we also characterized how the switch-on kinetics and the level of reporter expression varied in animals raised (and photoactivated) at different temperatures. In particular, we found that, at 29°C, the switch-on kinetics was 1.6-fold faster and the maximal level of His2B:RFP accumulation was 1.3-fold higher relative to those observed at 19 ± 1°C (Figures S1H and S1I). In addition, we found that, at a given temperature, the switch-on kinetics varied somewhat between different UAS reporters (Figure S1J).

To determine the switch-off kinetics of the ubi-Gal4$^{MagHigh}$ driver, we illuminated the tissue with 4 s pulses every minute for 1 h (491 nm, 0.5 mW) and recorded the subsequent dynamics of the UAS-His2B:RFP reporter. After reaching its maximal level at 7.2 ± 0.8 h, the His2B:RFP signal decreased by 10% at 9.3 ± 0.6 h after the end of the 491-nm illumination (Figures 1H and 1I). We then compared this decay kinetics with that of UAS-driven nls:Scarlet:PEST, expected to be rendered unstable by a proline, glutamic acid, serine, and threonine (PEST) stretch (Rechsteiner and Rogers, 1996). The nls:Scarlet:PEST signal was maximal at 7 ± 1 h and decreased by 10% at 9.2 ± 1 h after the end of the 491-nm illumination (Figures S2A and S2B), values that are similar to those observed with UAS-His2B:RFP. This suggests that the decrease in protein levels after returning to the dark is mainly driven by the switch-off kinetics of the MagHigh1 photoswitches. We found that a faster switch-off kinetics can be achieved by combining ubi-Gal4DBD:2xnMagHigh1 with the ubi-2xpMagFast1:AD transgene, albeit at the cost of lower signal intensity (Figures S2C–S2F). Taken together, our data establish that the ubi-Gal4$^{MagHigh}$ driver rapidly turns on ubiquitous gene expression upon 491-nm illumination within the context of a whole living animal and that the resulting protein accumulation is maintained for several hours after the end of 491-nm illumination.

## Spatial control of gene expression by local photoactivation

Having found that the ubi-Gal4$^{MagHigh}$ driver can be photoactivated at the tissue scale, we investigated whether it could be used to control gene expression locally, in a region of interest (ROI) and at a given developmental time. Using a spinning disc microscope, we found that a single pulse of 10 ms (0.5 mW) was sufficient to induce the accumulation of His2B:RFP in a tissue region, although this was in an area slightly larger than the illuminated field (Figure 2A; Video S2). The dynamics of His2B:RFP accumulation was comparable to that of the global tissue activation routines (Figures S2G and S2H). Hence, very short exposure routines suffice for local upregulation of gene expression. It has been previously reported that multiphoton illumination enables cellular resolution photoactivation of the Cry2/CIBN optogenetic module in *Drosophila* (Guglielmi et al., 2015). We found that 920 nm multiphoton illumination routines (40 scans, pixel dwell time of 0.76 μs at 25.2 mW) lasting a few minutes were sufficient to robustly activate His2B:RFP expression exclusively in the illuminated ROI (Figures 2B and 2C). By modulating the temporal and spatial pattern of illumination, we were able to achieve gene expression patterns in different ROI either simultaneously or sequentially, the latter enabling wave-like activation of gene expression (Figures 2C and 2D; Videos S3 and S4). Furthermore, by combining ubi-Gal4$^{MagHigh}$ and UAS-FLP, we achieved local excision of an FRT-flanked stop cassette, resulting in stable gene expression in a specific ROI (Figure S2I). Lastly, by varying the laser power (from 18.3 to 28.7 mW) or the number of illumination scans (from 20 to 50), we could modulate the number of His2B:RFP expressing cells and the levels of His2B:RFP within a ROI (Figures 2E and 2F). Accordingly, we could induce graded His2B:RFP expression within a tissue ROI (Figures S2J and S2K). Altogether, we conclude that photoactivation of the ubi-Gal4$^{MagHigh}$ driver constitutes a versatile platform for local activation of gene expression. We will subsequently refer to this optogenetic binary system as ShineGal4/UAS.

## ShineGal4 is effective in multiple tissues and at different life cycle stages

To further test the versatility and relevance of the ShineGal4/UAS system, we tested its ability to induce gene expression in other *Drosophila* tissues besides the notum and at various life cycle stages, including the adult. We found that ubi-Gal4$^{MagHigh}$ enables the expression of UAS reporters in the pupal wing upon global 488-nm illumination or local two photon illumination (Figures 3A and S3A). In addition, the ubi-Gal4$^{MagHigh}$ driver could be used to activate His2B:RFP expression in any chosen pupal histoblast nest (Figure 3B). Next, we investigated whether ubi-Gal4$^{MagHigh}$ could be used to activate gene expression in 3$^{rd}$ instar larvae. By adapting a protocol for imaging anesthetized larvae (Kakanj et al., 2020), we found that multiphoton illumination turned on His2B:RFP expression in a ROI of the wing disc pouch (Figures S3B and S3C). Furthermore, by specifically photoactivating the presumptive notum region of one of the two wing imaginal discs, we recovered strong His2B:RFP expression in the corresponding pupal hemi-notum, illustrating the possibility of gene activation on one side of the animal (Figures 3C and 3D). Remarkably, exposing pupae or 3$^{rd}$ instar larvae to ambient light or to 460 nm LED light was sufficient to induce gene expression in pupal tissues, imaginal discs, or the central nervous system of the larva (Figures S3D–S3G). We also tested the ability of ubi-Gal4$^{MagHigh}$ to induce gene expression in the early embryo and found that a 1 s pulse of 488 nm (0.2 mW) illumination in pre-gastrulating embryos was sufficient to promote His2B:RFP accumulation (Figures 3E, S3H, and S3I; Video S5). Lastly, we investigated whether the ShineGAL4/UAS system can promote gene expression in adults, using the follicular epithelium, the Malpighian tubules, and the gut as test cases. Except for the small R5 region of the posterior midgut region, the ubi-Gal4$^{MagHigh}$ photoactivation achieved strong gene expression, with low background being detectable in the absence of illumination (Figure S3J). Together, our data show that photoactivation of the ShineGal4/UAS system allows robust UAS-driven gene expression induction in multiple tissues at different life cycle stages in whole living animals.

## Making patterned Gal4 drivers light sensitive

We envision that it will be beneficial to light-induce gene expression (i) only in a subset of cells within a tissue; (ii) in a specific tissue; or (iii) in a given gene expression pattern in a large number of animals. We, therefore, set out to design pattern-specific

Please cite this article in press as: di Pietro et al., Rapid and robust optogenetic control of gene expression in *Drosophila*, Developmental Cell (2021), https://doi.org/10.1016/j.devcel.2021.11.016



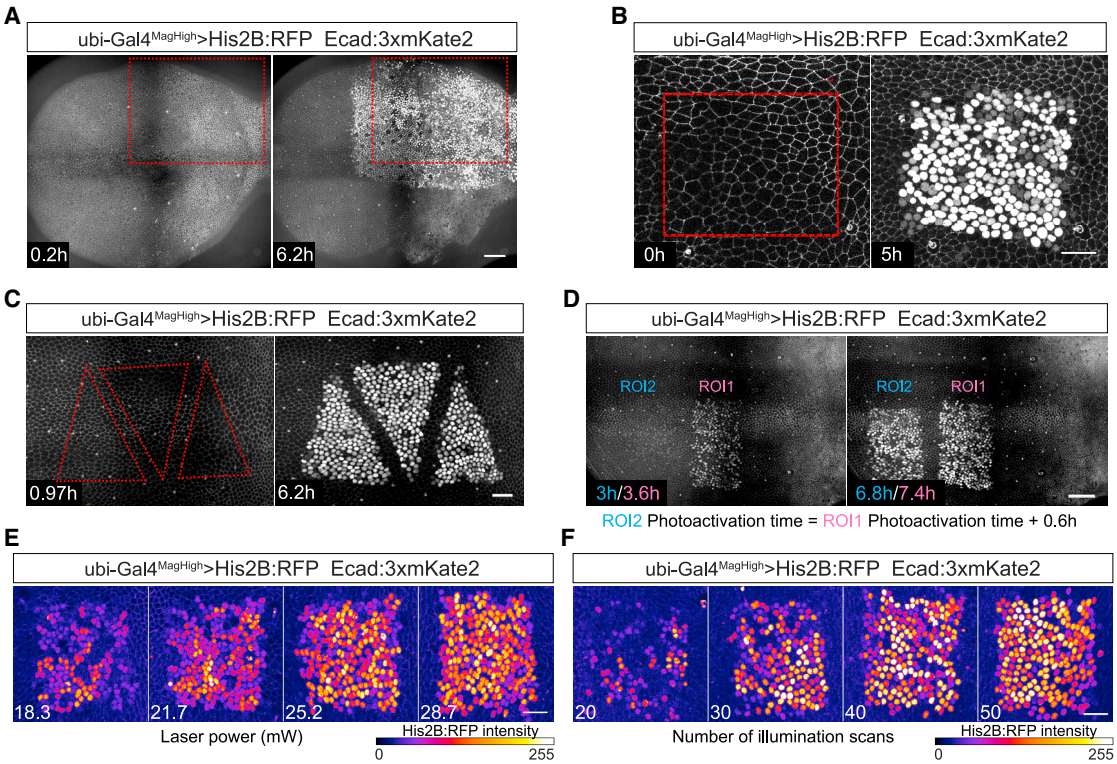


**Figure 2. Spatial control of gene expression by local photoactivation in the pupal notum**

Illumination settings used for photoactivation and imaging are given in Table S1A.

(A) Confocal images of Ecad:3xmKate2 and ubi-Gal4$^{MagHigh}$>His2B:RFP at 0.2 h and 6.2 h after a single 10 ms 491-nm illumination pulse in the indicated field of view (red dashed box). Time (h) is set to 0 at the end of the 491-nm illumination. See also Video S2. Light scattering might explain that the His2B:RFP expression region is slightly larger than the one of the 491-nm illuminated field.

(B) Confocal images of Ecad:3xmKate2 and ubi-Gal4$^{MagHigh}$>His2B:RFP prior to and 5 h after two photon 920-nm illumination in the indicated ROI (red dashed box). Time (h) is set to 0 at the end of the 920-nm illumination. The change in the ROI shape is due to the tissue deformations associated with morphogenesis.

(C) Confocal images of Ecad:3xmKate2 and ubi-Gal4$^{MagHigh}$>His2B:RFP upon two photon 920-nm illumination in multiple ROI (red dashed boxes). Time (h) is set to 0 at the end of the 920-nm illumination. See also Video S3.

(D) Confocal images of Ecad:3xmKate2 and ubi-Gal4$^{MagHigh}$>His2B:RFP upon sequential two photon 920-nm illumination in two different ROI. The ROI2 (blue) photoactivation was performed 0.6 h after the one of ROI1 (pink). Time (h) after the photoactivation of each ROI is indicated in their corresponding colors. See also Video S4.

(E) Confocal images of Ecad:3xmKate2 and ubi-Gal4$^{MagHigh}$>His2B:RFP 5 h after two photon 920-nm illumination at increasing laser power and constant number of illumination scans (40) in 4 different ROI. Images are projections in the plane of the nuclei, the AJ Ecad:3xmKate2 signal is not visible. All photoactivations shown were performed in the same notum epithelium.

(F) Confocal images of Ecad:3xmKate2 and ubi-Gal4$^{MagHigh}$>His2B:RFP 5 h after two photon 920-nm illumination at increasing number of illumination scans and constant laser power (25.2 mW) in 4 different ROI. Images are taken in the plane of the nuclei, the AJ Ecad:3xmKate2 signal is not visible. All photoactivations shown were performed in the same notum epithelium.

Scale bars: 50 μm (A and D) and 20 μm (B, C, E, and F).

See also Figure S2; Videos S2, S3, and S4; Table S1A.

ShineGal4 drivers. As a proof of principle, we combined the ubi-2xpMagHigh1:AD transgene with a Gal4DBD:2xnMagHigh1 gene controlled by the endogenous *wingless* (*wg*) promoter (Figure 4A); we called this bipartite driver wg-Gal4$^{MagHigh}$. We found that upon photoactivation in the notum or in the embryo, wg-Gal4$^{MagHigh}$ induced LifeAct:GFP accumulation in the expected *wg* expression domains (Figures 4B and 4C; Video S6). Using a similar approach, we also generated ush-Gal4$^{MagHigh}$ and mirr-Gal4$^{MagHigh}$ drivers (Figures S4A and S4B). Lastly, to leverage the very large collection of existing Gal4 drivers, we implemented a simple approach to render any existing Gal4 driver light sensitive using generic CRISPR/Cas9 guide RNA and targeting vectors (Figures S4C and S4D). Using this approach, we converted the wing pouch driver pdm2-Gal4 into a pdm2-Gal4$^{MagHigh}$ light-responsive driver (Figures 4D and S4E). Overall, these data show that new optogenetic drivers can be readily created to allow facile, spatially restricted activation of gene expression at defined experimental times.

## ShineGal4 as a tool to modulate gene function

We then investigated whether ShineGal4 is capable of generating gain- or loss-of-function phenotypes in whole animals or in specific tissue regions. First, we crossed the ubi-Gal4$^{MagHigh}$ driver to the UAS-ebony$^{dsRNA}$ transgene and raised the progeny in the dark or at ambient light from the 3$^{rd}$ instar larval stage onwards. Whereas the adult flies raised in the dark had a wild-type

Please cite this article in press as: di Pietro et al., Rapid and robust optogenetic control of gene expression in *Drosophila*, Developmental Cell (2021), https://doi.org/10.1016/j.devcel.2021.11.016



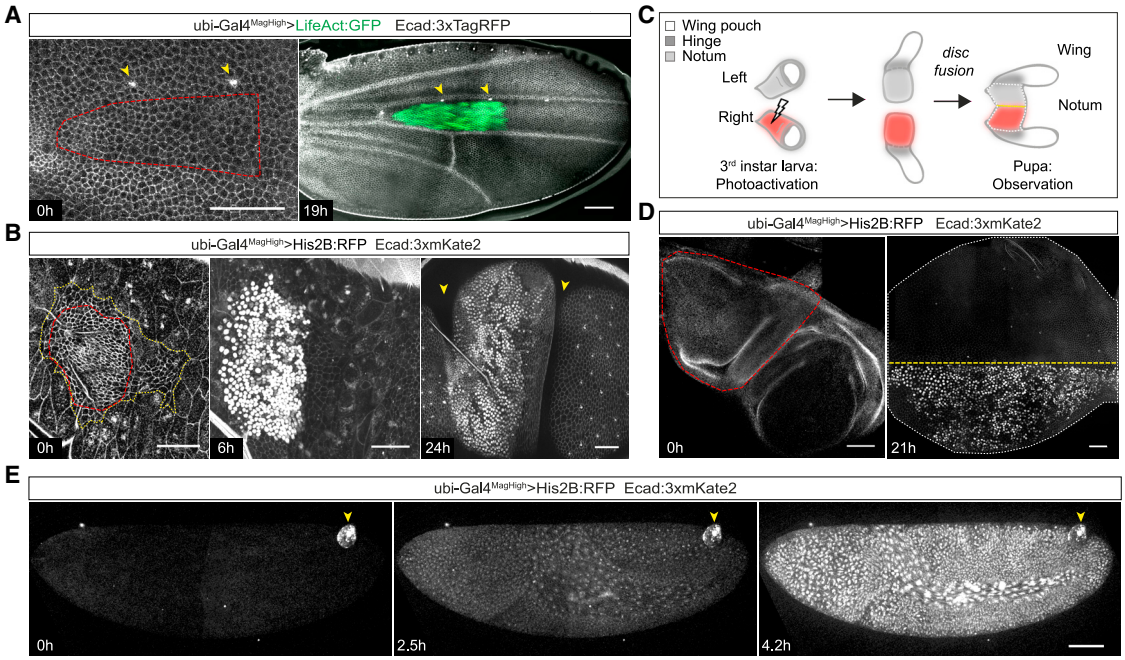


**Figure 3. ShineGal4 is effective in multiple tissues and at different life cycle stages**

Illumination settings used for photoactivation and imaging are given in Table S1A.

(A) Confocal images of Ecad:3xTagRFP (left and right) and ubi-Gal4$^{MagHigh}$>LifeAct:GFP (right) in a pupal wing prior to and 19 h after two photon 920-nm illumination in a ROI (red dashed line). The pupal wing undergoes extensive morphogenetic changes, explaining the changes in the ROI shape (Etournay et al., 2015). Yellow arrowheads: macrochaetae. Time (h) is set to 0 at the end of 920-nm illumination and corresponds to 16 hAPF.

(B) Confocal images of Ecad:3xmKate2 and ubi-Gal4$^{MagHigh}$>His2B:RFP in the pupal abdomen prior to, 6 h and 24 h after two photon 920-nm illumination in a ROI (red dashed line). During pupal development, the histoblast nests grow, expand, and fuse, accounting for the increased surface covered by the histoblast nest, while larval epithelial cells are lost by apoptosis (Ninov et al., 2009). Yellow dashed line: histoblast nest. Yellow arrowheads: segmental boundaries. The contrast is higher in the image at 0 h to better visualize Ecad:3xmKate2 signal and the histoblast nest cells.

(C) Schematics of the bilateral wing imaginal discs in a 3$^{rd}$ instar larva, highlighting the domains that, upon morphogenesis and fusion, give rise to the notum and wing tissues in the pupa. The strategy used to induce His2B:RFP expression in a pupal hemi-notum by local photoactivation in the presumptive notum region (red region) in a single larval wing imaginal disc is also outlined. White dashed line: pupal notum outline. Yellow dashed line: notum midline.

(D) Confocal images of Ecad:3xmKate2 and ubi-Gal4$^{MagHigh}$>His2B:RFP in a 3$^{rd}$ instar larva wing imaginal disc before photoactivation (left) and of the notum of a pupa upon photoactivation in the 3$^{rd}$ instar larva imaginal disc (right). The red dashed line in the left panel indicates the presumptive notum region where photoactivation was typically performed. White dashed line: pupal notum outline. Yellow dashed line: notum midline. Time (h) is set to 0 at the end of 920-nm illumination.

(E) Time-lapse images of Ecad:3xmKate2 and ubi-Gal4$^{MagHigh}$>His2B:RFP in an embryo following 488-nm illumination. Time (h) is set to 0 at the end of the 488-nm illumination and corresponds to the blastoderm stage. Note that the Ecad:3xmKate2 is too dim at these stages to be clearly observed. See also Video S5 and Figure S3H. Yellow arrowheads: debris on top of the embryo, probably corresponding to a chorion fragment.

Scale bars: 50μm.

See also Figure S3; Video S5; Table S1A.

(wt) body color, the ones raised in ambient light exhibited an *ebony* mutant phenotype (Figures 5A and S5A). Next, we aimed at creating a light-inducible loss-of-function allele of *vestigial* (*vg*) by combining a *vg* conditional allele (coding sequence flanked by FRT sites; FRT-Vg-FRT) with ubi-Gal4$^{MagHigh}$ and UAS-FLP. We found that ambient light was sufficient to generate a full *vg* loss-of-function phenotype, as manifested by the absence of wings (Figures 5B and S5B). Because ubi-Gal4$^{MagHigh}$ can induce different levels of gene expression by tuning the illumination routine (Figures 2E and 2F), we then investigated whether a phenotypic series could be generated. First, we established that increasing the duration of exposure to 460 nm LED blue light resulted in increased levels of reporter gene expression in pupae (Figures S5C and S5D). Then, we used ubi-Gal4$^{MagHigh}$ to induce *Dpp* overexpression at the pupal stage, which is known to cause ectopic vein formation in the adult (De Celis, 1997). Whereas the animals raised in the dark exhibited a normal vein pattern, those exposed to light showed an ectopic vein phenotype that got stronger with longer illumination (Figures 5C and 5D). Together, these experiments show that ShineGal4 allows the modulation of gene activity at the animal scale to generate loss- and gain-of-function phenotypes.

The significance of functional studies is greatly enhanced by (i) systematic modulation of gene expression in the same tissue regions in multiple experiments and/or (ii) comparison of gain- and loss-of-function phenotypes between bilateral symmetric organs. We therefore investigated the ability of ShineGal4 to induce gain or loss-of-function phenotypes in a given tissue ROI at a timescale of hours. As an example of gain of function, we manipulated cell proliferation in the pupal notum. We used the ubi-Gal4$^{MagHigh}$ driver and multiphoton illumination to activate the expression of the G1/S CyclinE (CycE) in a defined

Please cite this article in press as: di Pietro et al., Rapid and robust optogenetic control of gene expression in *Drosophila*, Developmental Cell (2021), https://doi.org/10.1016/j.devcel.2021.11.016



CellPress
OPEN ACCESS

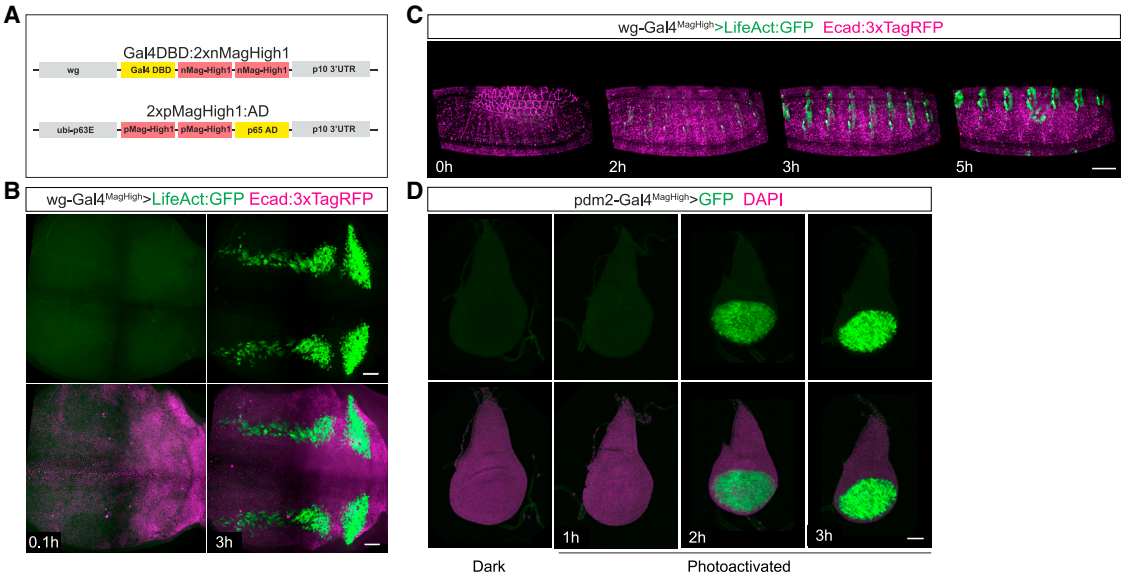


**Figure 4. Making patterned Gal4 drivers light sensitive**

Illumination settings used for photoactivation and imaging are given in Table S1A.

(A) Schematic of the wg-Gal4DBD:2xnMagHigh1 and ubi-2xpMagHigh1:AD transgenes referred to as wg-Gal4$^{MagHigh}$.

(B) Time-lapse images of Ecad:3xTagRFP (bottom) and wg−Gal4$^{MagHigh}$>LifeAct:GFP (top and bottom) in the notum epithelium of a pupa upon 491-nm illumination. Time (h) is set to 0 at the start of 491-nm illumination. See also Video S6.

(C) Time-lapse images of Ecad:3xTagRFP and wg−Gal4$^{MagHigh}$>LifeAct:GFP during 488-nm illumination in an embryo from stage 13 onwards. Time (h) is set to 0 at the start of the 488-nm illumination.

(D) Confocal images of DAPI (bottom) and pdm2-Gal4$^{MagHigh}$>GFP (top and bottom) in wing imaginal discs dissected from early 3$^{rd}$ instar larva that were either kept in the dark (left) or exposed to blue light during 5 min and fixed at the indicated times after photoactivation. See also Figures S4C–S4E.

Scale bars: 50 μm.

See also Figure S4; Video S6; Table S1A.

ROI and compared its resulting proliferation rate with that of the contralateral ROI (Figure 5E). Upon completing one cell cycle, we found that cells in the photoactivated ROI re-entered the cell cycle, whereas the contralateral did not, establishing that cell proliferation can be spatially controlled by ShineGal4 (Figures 5F, 5G, and S5E; Video S7). To test our ability to achieve loss of function in a given tissue region, we aimed at locally abrogating Myosin II (MyoII) function in the pupal notum. In one approach, overexpression of a dominant-negative form of the Myosin II heavy chain (Zip$^{DN}$:YFP; Dawes-Hoang et al., 2005) promoted an increase in cell apical area within 8 h in the activated ROI relative to the control contralateral cells (Figures 5H, 5J, and S5F). Such increase was sustained for at least 24 h after illumination (Figures S5G and S5H), indicating that ShineGal4 enables to investigate both the short- and long-term consequences of local dominant-negative form expression. In a separate approach, we optogenetically expressed deGradFP to promote MyoII:GFP degradation (Caussinus et al., 2011). Local expression of deGradFP in animals expressing MyoII:GFP as the only source of MyoII (Ambrosini et al., 2019) led to the formation of bright MyoII:GFP clusters within 4 h after photoactivation (Figure S5I). Within an additional 4 h, MyoII:GFP signal became almost completely absent from the apical cell cortex (Figures 5I and S5I) and the cell apical area was increased relative to that in the contralateral region (Figures 5I, 5K, S5J, and S5K). Together, these results establish that ShineGal4/UAS enables global and local modulations of gene activity at given developmental times.

## DISCUSSION

### ShineGal4/UAS as a plug-and-play optogenetic system

Over the years, the Gal4/UAS system has developed into a powerful tool to control gene expression and decipher gene function. Building on the Magnet photoswitches to develop ShineGal4, we rendered the Gal4/UAS system light dependent, thus further expanding its range of experimental opportunities in whole living organisms. We show that ShineGal4 enables efficient and robust gene expression in multiple tissues and life cycle stages. It readily combines with the FLP/FRT system (Xu and Rubin, 1993) to generate somatic clones at high temporal and spatial resolution. Furthermore, ShineGal4 can also leverage existing Gal4 drivers to activate gene expression in genetically determined patterns at experimentally chosen times. The availability of optogenetic drivers of different switch-off kinetics, slow with ubi-Gal4$^{MagHigh}$ or fast with ubi-Gal4$^{MagFast1}$ drivers, will further refine the opportunities for temporal modulation of gene expression. The ShineGal4/UAS system opens up a wide range of experimental avenues to explore gene function locally and temporally in whole animals.

By enabling light-dependent induction of any UAS transgene, possibly in any tissue, the versatility of ShineGal4 complements previously established optogenetic approaches (Johnson and Toettcher, 2019; López-Gay et al., 2020; De Renzis, 2020; Toettcher et al., 2011; Viswanathan et al., 2019), which were designed for specific purposes, such as the fast modulation of

Please cite this article in press as: di Pietro et al., Rapid and robust optogenetic control of gene expression in *Drosophila*, Developmental Cell (2021), https://doi.org/10.1016/j.devcel.2021.11.016



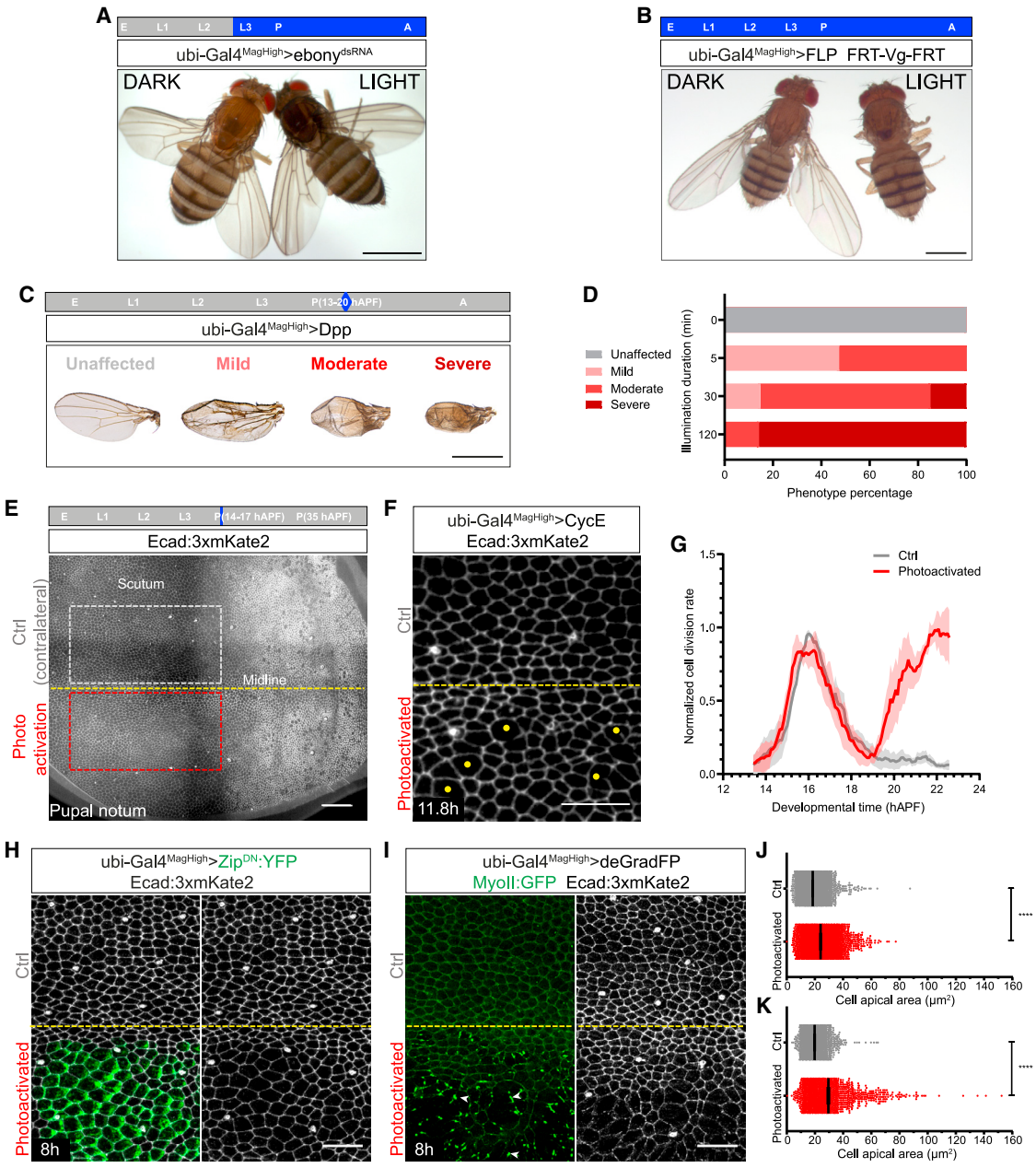


**Figure 5. ShineGal4 as a tool to modulate gene function**

Illumination settings used for photoactivation and imaging are given in Table S1A. The illumination routine is indicated at the top of the panels (E: embryo, L1, L2, L3: 1st, 2nd, 3rd instar larva, respectively, P: pupa, A: adult). Unless otherwise stated, images were taken in the notum epithelium. N, number of animals.

(A) Image of ubi-Gal4$^{MagHigh}$>ebony$^{dsRNA}$ adult flies either kept in the dark (left) or exposed to ambient light from the 3rd instar larva stage onwards (right). See also Figure S5A.

(B) Image of ubi-Gal4$^{MagHigh}$>FLP adult flies carrying a *vg* allele flanked by FRT sites (FRT-Vg-FRT) either kept in the dark (left) or exposed to ambient light (right) throughout their whole development. See also Figure S5B.

(C) Images of wings from ubi-Gal4$^{MagHigh}$>Dpp animals either kept in the dark or exposed to 460 nm LED illumination for 5, 30, or 120 min between 13 and 20 hAPF to illustrate the different phenotypic classes observed.

(D) Histogram of the percentage of each phenotypic class for the experiment shown in (C). N = 26 (0 min), 19 (5 min), 27 (30 min), and 15 (120 min).

(E) Confocal image of Ecad:3xmKate2 in the pupal notum showing the relative positions of the 920 nm photoactivated ROI (red) and contralateral control regions (Ctrl, gray) to illustrate the strategy used in experiments shown in (F)–(K). Yellow dashed line: midline.

(F) Confocal image of Ecad:3xmKate2 in a ubi-Gal4$^{MagHigh}$>CycE notum in the photoactivated and contralateral control regions at 11.8 h (21 hAPF) after two photon 920 nm photoactivation. In the most anterior part of the notum (scutum), cells are initially blocked in G2 and most cells divide once between 14 and 18 hAPF and then enter quiescence (Bosveld et al., 2012, 2016; Guirao et al., 2015). In the photoactivated region, cell divisions (yellow dots) can be observed. Yellow dashed line: midline.

*(legend continued on next page)*

MyoII function or ERK activity. Although these approaches were successful and achieved faster kinetics, they tended to require a significant investment in design and optimization. We view ShineGal4/UAS as a plug-and-play system that will be readily implemented for a wide range of applications and with minimal effort. In addition, our results suggest that the Magnet photoswitches could be used to design other binary optogenetic systems such as Q/QUAS or LexA/LexO without leakiness in dark conditions (Chan et al., 2015; Potter et al., 2010; Yagi et al., 2010). One could also envision using the Magnet photoswitches to build additional *Drosophila* optogenetic tools to modulate gene function such as CRISPR/deadCas9 or optogenetic FLP or Cre systems as shown in mammalian systems (Jung et al., 2019; Kawano et al., 2016; Weinberg et al., 2019). Lastly, our findings suggest that Magnet photoswitches or their more stable enhanced Magnets (eMagnet; Benedetti et al., 2020) could be used to design transgenic binary systems in other model systems.

In conclusion, we propose that, combined with the ever-growing catalog of UAS reporters and genome-wide collections ranging from dsRNA (Dietzl et al., 2007; Kaya-Çopur and Schnorrer, 2016; Zirin et al., 2020) to single-strand guide RNA-Cas9 (Port et al., 2020) libraries, the ShineGAL4/UAS system enriches the *Drosophila* genetic toolkit by opening the possibility to control gene expression with an exquisite temporal and spatial resolution.

### Limitations of the study

So far, we have only determined the switch-on and -off kinetics of the ubi-Gal4$^{MagHigh}$, ubi-Gal4$^{Mag}$ and ubi-Gal4$^{MagFast1}$ drivers in the notum. Characterizing their kinetics in a variety of tissues remains to be done. We found that the faster ubi-Gal4$^{MagFast1}$ switch-off kinetics came at the expense of lower levels of gene activation. Perhaps this could be overcome by further increasing the transgene expression level or the number of MagFast1 photoswitch repeats. We have used complementary approaches to generate several patterned ShineGal4 drivers. In one, which can be used to convert any existing driver line light sensitive, we micro-injected generic CRISPR/Cas9 guide RNA and targeting vectors in embryos of the appropriate Gal4-expressing strain. Such conversion could be achieved without the need for injection by adapting the E-Golic+ approach for gene conversion (Chen et al., 2020). So far, we have achieved patterned optogenetic drivers by combining Gal4DBD:2xnMagHigh (Figure 1) expressed from a patterned promoter with ubi-2xpMagHigh1:AD, which is ubiquitously expressed. Further work will be needed to assess whether the two elements of ShineGal4 can be both expressed from patterned promoters to further refine the ShineGal4 activation domain upon global light exposure.

## STAR★METHODS

Detailed methods are provided in the online version of this paper and include the following:

- KEY RESOURCES TABLE
- RESOURCE AVAILABILITY
  - Lead contact
  - Materials availability
  - Data and code availability
- EXPERIMENTAL MODEL AND SUBJECT DETAILS
  - Fly stocks and genetics
- METHOD DETAILS
  - Molecular biology and transgenesis
  - Animal mounting for imaging
  - Larva and adult tissue dissection and staining
  - Microscopy and photoactivation
  - Photoactivation in whole animals
  - Figures preparation
- QUANTIFICATION AND STATISTICAL ANALYSIS
  - Quantifications
  - Statistics

### SUPPLEMENTAL INFORMATION

Supplemental information can be found online at https://doi.org/10.1016/j.devcel.2021.11.016.

### ACKNOWLEDGMENTS

We thank G. Perez-Mockus and Z. Wang for sharing the unpublished UAS-nls:Scarlet:PEST and the Ecad:3xiRFP670 lines, respectively; J. Kurth (FCI) for *Drosophila* injection; J. van den Ameele for advice on optogenetic systems; A. Dauphin and O. Renaud for laser power measurements; M. Balakireva for information on gene expression patterns in the notum; M. Lambers for help with molecular cloning and initial characterization of the iLID/SspB Gal4 system; Z. Wang for testing a GAVPO system in *Drosophila*; P. Kakanj for help with anesthetized larva imaging; M. Gho, Y. Hong, D. Kiehart, M. Suzanne, the Bloomington Stock Centre, Vienna Drosophila Resource Center, Transgenic RNAi Project at Harvard Medical School, and Kyoto Stock Center; and

(G) Graph of the normalized cell division rate (±SEM, N = 3) in photoactivated (red) and control contralateral regions (gray) for the experiment shown in (F). In total, 784 and 790 cells were initially tracked in the photoactivated and contralateral regions, respectively. The multiphoton photoactivations were performed at around 12 hAPF. Values are normalized to the maximal value of each condition. See also Figure S5E and Video S7.

(H) Confocal image of Ecad:3xmKate2 (left and right) and ubi-Gal4$^{MagHigh}$>Zip$^{DN}$:YFP (left) in the photoactivated and control contralateral regions at 8 h (25 hAPF) after two photon 920 nm photoactivation. Yellow dashed line: midline.

(I) Confocal image of MyoII:GFP (left) and Ecad:3xmKate2 (right) in a ubi-Gal4$^{MagHigh}$>deGradFP pupal notum within the photoactivated and control contralateral regions at 8 h (24 hAPF) after two photon 920 nm photoactivation. UAS-deGradFP is based on a GFP nanobody fused to a Slimb box degrading the GFP-tagged protein bound by this nanobody (Caussinus et al., 2011). White arrowheads: MyoII:GFP aggregates (Caussinus et al., 2011). Yellow dashed line: midline. See also Figures S5I and S5K.

(J) Graph of cell apical areas for the experiment performed in (H) (N = 5; 4,876; and 4,177 cells in the control and photoactivated regions, respectively). p value < 0.0001. See also Figures S5F–S5H.

(K) Graph of cell apical areas for the experiment performed in (I) (N = 5; 1,866; and 1,450 cells in the control and photoactivated regions, respectively). p value < 0.0001.

Scale bars: 1 mm (A, B, and C), 50 μm (E), and 20 μm (F, H, and I).

See also Figure S5; Video S7; Table S1A.

the PICT-IBiSA@BDD imaging facility of the Institut Curie (member of the French National Research Infrastructure France-BioImaging, ANR-10-INBS-04). We thank ERC Advanced (TiMoprh, 340784), Fondation ARC contre le cancer (SL220130607097), ANR Migrafolds (ANR-18-CE13-0021), ANR Labex DEEP (11-LBX-0044, PSL ANR-10-IDEX-0001-02), Leverhulme Trust, and St John's College for funding grants. This work was supported by a Wellcome Trust Investigator award (206341/Z/17/Z to J.P.V.) and by the Francis Crick Institute, which receives its core funding from Cancer Research UK (FC001204), the UK Medical Research Council (FC001204), and the Wellcome Trust (FC001204). F.d.P. is supported by a FRM post-doctoral fellowship (SPF20170938661). S.H. was supported by an EMBO Long Term Fellowship (ALTF1156-2015) and the Francis Crick Institute.

## AUTHORS CONTRIBUTIONS

Conceptualization, F.d.P., S.H., F.B., C.A., J-P.V., and Y.B.; formal analysis, F.d.P., L.S., and S.H.; funding acquisition, F.d.P., S.H., J.P.V., and Y.B.; investigation, F.d.P., S.H., A.H., F.B., C.A., and Y.B.; methodology, F.d.P., S.H., F.B., C.A., J-P.V., and Y.B.; project administration, Y.B. and J.P.V.; resources, F.d.P., S.H., A.H., C.A., S.P., and A.J.; software, L.S. and V.K.; supervision, Y.B. and J.P.V.; visualization, F.d.P., S.H., A.H., and Y.B.; writing—original draft, F.d.P. and Y.B.; writing—review and editing, F.d.P., Y.B., S.H., F.B., C.A., A.H., and J-P.V.

## DECLARATION OF INTERESTS

Yohanns Bellaiche is a Developmental Cell advisory board member.

Received: May 27, 2021
Revised: October 13, 2021
Accepted: November 15, 2021
Published: December 7, 2021

## REFERENCES

Adolfi, A., Pondeville, E., Lynd, A., Bourgouin, C., and Lycett, G.J. (2018). Multi-tissue GAL4-mediated gene expression in all *Anopheles gambiae* life stages using an endogenous polyubiquitin promoter. Insect Biochem. Mol. Biol. *96*, 1–9.

Alexandre, C., Baena-Lopez, A., and Vincent, J.P. (2014). Patterning and growth control by membrane-tethered wingless. Nature *505*, 180–185.

Ambrosini, A., Rayer, M., Monier, B., and Suzanne, M. (2019). Mechanical function of the nucleus in force generation during epithelial morphogenesis. Dev. Cell *50*, 197–211, e5.

Baena-Lopez, L.A., Alexandre, C., Mitchell, A., Pasakarnis, L., and Vincent, J.-P. (2013). Accelerated homologous recombination and subsequent genome modification in *Drosophila*. Development *140*, 4818–4825.

Benedetti, L., Marvin, J.S., Falahati, H., Guillén-Samander, A., Looger, L.L., and De Camilli, P. (2020). Optimized vivid-derived magnets photodimerizers for subcellular optogenetics in mammalian cells. Elife *9*, e63230.

Bischof, J., Maeda, R.K., Hediger, M., Karch, F., and Basler, K. (2007). An optimized transgenesis system for *Drosophila* using germ-line-specific φC31 integrases. Proc. Natl. Acad. Sci. USA *104*, 3312–3317.

Bosveld, F., Bonnet, I., Guirao, B., Tlili, S., Wang, Z., Petitalot, A., Marchand, R., Bardet, P.-L., Marcq, P., Graner, F., and Bellaïche, Y. (2012). Mechanical control of morphogenesis by Fat/Dachsous/Four-Jointed planar cell polarity pathway. Science *336*, 724–727.

Bosveld, F., Markova, O., Guirao, B., Martin, C., Wang, Z., Pierre, A., Balakireva, M., Gaugue, I., Ainslie, A., Christophorou, N., et al. (2016). Epithelial tricellular junctions act as interphase cell shape sensors to orient mitosis. Nature *530*, 495–498.

Brand, A.H., and Perrimon, N. (1993). Targeted gene expression as a means of altering cell fates and generating dominant phenotypes. Development *118*, 401–415.

Carey, M., Kakidani, H., Leatherwood, J., Mostashari, F., and Ptashne, M. (1989). An amino-terminal fragment of GAL4 binds DNA as a dimer. J. Mol. Biol. *209*, 423–432.

Caussinus, E., Kanca, O., and Affolter, M. (2011). Fluorescent fusion protein knockout mediated by anti-GFP nanobody. Nat. Struct. Mol. Biol. *19*, 117–121.

Caygill, E.E., and Brand, A.H. (2016). The GAL4 system: A versatile system for the manipulation and analysis of gene expression. Methods Mol. Biol. *1478*, 33–52.

Chan, Y.B., Alekseyenko, O.V., and Kravitz, E.A. (2015). Optogenetic control of gene expression in Drosophila. PLoS One *10*, e0138181.

Chen, H.M., Yao, X., Ren, Q., Chang, C.C., Liu, L.Y., Miyares, R.L., and Lee, T. (2020). Enhanced Golic+: highly effective CRISPR gene targeting and transgene HACKing in *Drosophila*. Development *147*, 1–9.

Classen, A.K., Aigouy, B., Giangrande, A., and Eaton, S. (2008). Imaging Drosophila pupal wing morphogenesis. Methods Mol. Biol. *420*, 265–275.

Curran, S., Strandkvist, C., Bathmann, J., de Gennes, M., Kabla, A., Salbreux, G., and Baum, B. (2017). Myosin II controls junction fluctuations to guide epithelial tissue ordering. Dev. Cell *43*, 480–492, e6.

David, N.B., Martin, C.A., Segalen, M., Rosenfeld, F., Schweisguth, F., and Bellaïche, Y. (2005). Drosophila Ric-8 regulates Gαi cortical localization to promote Gαi-dependent planar orientation of the mitotic spindle during asymmetric cell division. Nat. Cell Biol. *7*, 1083–1090.

Dawes-Hoang, R.E., Parmar, K.M., Christiansen, A.E., Phelps, C.B., Brand, A.H., and Wieschaus, E.F. (2005). Folded gastrulation, cell shape change and the control of myosin localization. Development *132*, 4165–4178.

De Celis, J.F. (1997). Expression and function of decapentaplegic and thick veins during the differentiation of the veins in the Drosophila wing. Development *124*, 1007–1018.

de Mena, L., and Rincon-Limas, D.E. (2020). PhotoGal4: A versatile light-dependent switch for spatiotemporal control of gene expression in Drosophila explants. iScience *23*, 101308.

de Mena, L., Rizk, P., and Rincon-Limas, D.E. (2018). Bringing light to transcription: the optogenetics repertoire. Front. Genet. *9*, 518. https://doi.org/10.3389/fgene.2018.00518.

De Renzis, S. (2020). Morphogenesis: guiding embryonic development with light. Curr. Biol. *30*, R998–R1001.

Dejima, K., Kanai, M.I., Akiyama, T., Levings, D.C., and Nakato, H. (2011). Novel contact-dependent bone morphogenetic protein (BMP) signaling mediated by heparan sulfate proteoglycans. J. Biol. Chem. *286*, 17103–17111.

Del Valle Rodríguez, A., Didiano, D., and Desplan, C. (2011). Power tools for gene expression and clonal analysis in *Drosophila*. Nat. Methods *9*, 47–55.

Dietzl, G., Chen, D., Schnorrer, F., Su, K.C., Barinova, Y., Fellner, M., Gasser, B., Kinsey, K., Oppel, S., Scheiblauer, S., et al. (2007). A genome-wide transgenic RNAi library for conditional gene inactivation in *Drosophila*. Nature *448*, 151–156.

Etournay, R., Popović, M., Merkel, M., Nandi, A., Blasse, C., Aigouy, B., Brandl, H., Myers, G., Salbreux, G., Jülicher, F., et al. (2015). Interplay of cell dynamics and epithelial tension during morphogenesis of the *Drosophila* pupal wing. Elife *4*, e07090.

Evans, C.J., Olson, J.M., Ngo, K.T., Kim, E., Lee, N.E., Kuoy, E., Patananan, A.N., Sitz, D., Tran, P.T., Do, M.T., et al. (2009). G-TRACE: rapid Gal4-based cell lineage analysis in *Drosophila*. Nat. Methods *6*, 603–605.

Founounou, N., Loyer, N., and Le Borgne, R. (2013). Septins regulate the contractility of the actomyosin ring to enable adherens junction remodeling during cytokinesis of epithelial cells. Dev. Cell *24*, 242–255.

Gehrig, S., Macpherson, J.A., Driscoll, P.C., Symon, A., Martin, S.R., MacRae, J.I., Kleinjung, J., Fraternali, F., and Anastasiou, D. (2017). An engineered photoswitchable mammalian pyruvate kinase. FEBS J *284*, 2955–2980.

Gibson, D.G., Young, L., Chuang, R.Y., Venter, J.C., Hutchison, C.A., and Smith, H.O. (2009). Enzymatic assembly of DNA molecules up to several hundred kilobases. Nat. Methods *6*, 343–345.

Groth, A.C., Fish, M., Nusse, R., and Calos, M.P. (2004). Construction of transgenic Drosophila by using the site-specific integrase from phage φC31. Genetics *166*, 1775–1782.

Guglielmi, G., Barry, J.D., Huber, W., and De Renzis, S. (2015). An optogenetic method to modulate cell contractility during tissue morphogenesis. Dev. Cell *35*, 646–660.

Guirao, B., Rigaud, S.U., Bosveld, F., Bailles, A., López-Gay, J., Ishihara, S., Sugimura, K., Graner, F., and Bellaïche, Y. (2015). Unified quantitative characterization of epithelial tissue development. eLife *4*, e08519.

Guntas, G., Hallett, R.A., Zimmerman, S.P., Williams, T., Yumerefendi, H., Bear, J.E., and Kuhlman, B. (2015). Engineering an improved light-induced dimer (iLID) for controlling the localization and activity of signaling proteins. Proc. Natl. Acad. Sci. USA *112*, 112–117.

He, L., Binari, R., Huang, J., Falo-Sanjuan, J., and Perrimon, N. (2019). In vivo study of gene expression with an enhanced dual-color fluorescent transcriptional timer. eLife *8*, 1–20.

Herszterg, S., Leibfried, A., Bosveld, F., Martin, C., and Bellaiche, Y. (2013). Interplay between the dividing cell and its neighbors regulates adherens junction formation during cytokinesis in epithelial tissue. Dev. Cell *24*, 256–270.

Huang, J., Zhou, W., Dong, W., Watson, A.M., and Hong, Y. (2009). From the Cover: directed, efficient, and versatile modifications of the Drosophila genome by genomic engineering. Proc. Natl. Acad. Sci. USA *106*, 8284–8289.

Jenett, A., Rubin, G.M., Ngo, T.T.B., Shepherd, D., Murphy, C., Dionne, H., Pfeiffer, B.D., Cavallaro, A., Hall, D., Jeter, J., et al. (2012). A GAL4-driver line resource for *Drosophila* neurobiology. Cell Rep *2*, 991–1001.

Johnson, H.E., and Toettcher, J.E. (2019). Signaling dynamics control cell fate in the early Drosophila embryo. Dev. Cell *48*, 361–370, e3.

Jung, H., Kim, S.W., Kim, M., Hong, J., Yu, D., Kim, J.H., Lee, Y., Kim, S., Woo, D., Shin, H.S., et al. (2019). Noninvasive optical activation of Flp recombinase for genetic manipulation in deep mouse brain regions. Nat. Commun. *10*, 314.

Kakanj, P., Eming, S.A., Partridge, L., and Leptin, M. (2020). Long-term in vivo imaging of *Drosophila* larvae. Nat. Protoc. *15*, 1158–1187.

Kawakami, K., Asakawa, K., Hibi, M., Itoh, M., Muto, A., and Wada, H. (2016). Gal4 driver transgenic zebrafish: powerful tools to study developmental biology, organogenesis, and neuroscience. Adv. Genet. *95*, 65–87.

Kawano, F., Okazaki, R., Yazawa, M., and Sato, M. (2016). A photoactivatable Cre-loxP recombination system for optogenetic genome engineering. Nat. Chem. Biol. *12*, 1059–1064.

Kawano, F., Suzuki, H., Furuya, A., and Sato, M. (2015). Engineered pairs of distinct photoswitches for optogenetic control of cellular proteins. Nat. Commun. *6*, 6256.

Kaya-Çopur, A., and Schnorrer, F. (2016). A guide to genome-wide in vivo RNAi applications in *Drosophila*. Methods Mol. Biol. *1478*, 117–143.

Kennedy, M.J., Hughes, R.M., Peteya, L.A., Schwartz, J.W., Ehlers, M.D., and Tucker, C.L. (2010). Rapid blue-light-mediated induction of protein interactions in living cells. Nat. Methods *7*, 973–975.

Kvon, E.Z., Kazmar, T., Stampfel, G., Yáñez-Cuna, J.O., Pagani, M., Schernhuber, K., Dickson, B.J., and Stark, A. (2014). Genome-scale functional characterization of Drosophila developmental enhancers in vivo. Nature *512*, 91–95.

Landis, G.N., Salomon, M.P., Keroles, D., Brookes, N., Sekimura, T., and Tower, J. (2015). The progesterone antagonist mifepristone/RU486 blocks the negative effect on life span caused by mating in female *Drosophila*. Aging (Albany NY) *7*, 53–69.

Langevin, J., Le Borgne, R., Rosenfeld, F., Gho, M., Schweisguth, F., and Bellaïche, Y. (2005). Lethal giant larvae controls the localization of Notch-signaling regulators Numb, neuralized, and Sanpodo in *Drosophila* sensory-organ precursor cells. Curr. Biol. *15*, 955–962.

Levayer, R., Dupont, C., and Moreno, E. (2016). Tissue crowding induces caspase-dependent competition for space. Curr. Biol. *26*, 670–677.

Li, M.Z., and Elledge, S.J. (2012). SLIC: a method for sequence- and ligation-independent cloning. Methods Mol. Biol. *852*, 51–59.

Liu, H., Gomez, G., Lin, S., Lin, S., and Lin, C. (2012). Optogenetic control of transcription in zebrafish. PLoS One *7*, e50738.

Lo, C.-A., Kays, I., Emran, F., Lin, T.J., Cvetkovska, V., and Chen, B.E. (2015). Quantification of protein levels in single living cells. Cell Rep *13*, 2634–2644.

López-Gay, J.M., Nunley, H., Spencer, M., di Pietro, F., Guirao, B., Bosveld, F., Markova, O., Gaugue, I., Pelletier, S., Lubensky, D.K., and Bellaïche, Y. (2020). Apical stress fibers enable a scaling between cell mechanical response and area in epithelial tissue. Science *370*, eabb2169.

McGuire, S.E., Le, P.T., and Davis, R.L. (2001). The role of Drosophila mushroom body signaling in olfactory memory. Science *293*, 1330–1333.

McGuire, S.E., Le, P.T., Osborn, A.J., Matsumoto, K., and Davis, R.L. (2003). Spatiotemporal rescue of memory dysfunction in Drosophila. Science *302*, 1765–1768.

Mruk, K., Ciepla, P., Piza, P.A., Alnaqib, M.A., and Chen, J.K. (2020). Targeted cell ablation in zebrafish using optogenetic transcriptional control. Development *147*, dev183640.

Nicholson, L., Singh, G.K., Osterwalder, T., Roman, G.W., Davis, R.L., and Keshishian, H. (2008). Spatial and temporal control of gene expression in Drosophila using the inducible geneSwitch GAL4 system. I. Screen for larval nervous system drivers. Genetics *178*, 215–234.

Ninov, N., Manjón, C., and Martín-Blanco, E. (2009). Dynamic control of cell cycle and growth coupling by ecdysone, egfr, and PI3K signaling in *Drosophila* histoblasts. PLoS Biol *7*, e1000079.

Pathak, G.P., Spiltoir, J.I., Höglund, C., Polstein, L.R., Heine-Koskinen, S., Gersbach, C.A., Rossi, J., and Tucker, C.L. (2017). Bidirectional approaches for optogenetic regulation of gene expression in mammalian cells using *Arabidopsis* cryptochrome 2. Nucleic Acids Res *45*, e167.

Pfeiffer, B.D., Ngo, T.T.B., Hibbard, K.L., Murphy, C., Jenett, A., Truman, J.W., and Rubin, G.M. (2010). Refinement of tools for targeted gene expression in Drosophila. Genetics *186*, 735–755.

Pfeiffer, B.D., Truman, J.W., and Rubin, G.M. (2012). Using translational enhancers to increase transgene expression in *Drosophila*. Proc. Natl. Acad. Sci. USA *109*, 6626–6631.

Pinheiro, D., Hannezo, E., Herszterg, S., Bosveld, F., Gaugue, I., Balakireva, M., Wang, Z., Cristo, I., Rigaud, S.U., Markova, O., and Bellaïche, Y. (2017). Transmission of cytokinesis forces via E-cadherin dilution and actomyosin flows. Nature *545*, 103–107.

Poernbacher, I., Crossman, S., Kurth, J., Nojima, H., Baena-Lopez, A., Alexandre, C., and Vincent, J.P. (2019). Lessons in genome engineering: opportunities, tools and pitfalls. BioRxiv. https://doi.org/10.1101/710871.

Port, F., Chen, H.M., Lee, T., and Bullock, S.L. (2014). Optimized CRISPR/Cas tools for efficient germline and somatic genome engineering in *Drosophila*. Proc. Natl. Acad. Sci. USA *111*, E2967–E2976.

Port, F., Strein, C., Stricker, M., Rauscher, B., Heigwer, F., Zhou, J., Beyersdörffer, C., Frei, J., Hess, A., Kern, K., et al. (2020). A large-scale resource for tissue-specific CRISPR mutagenesis in *Drosophila*. Elife *9*, e53865.

Potter, C.J., Tasic, B., Russler, E.V., Liang, L., and Luo, L. (2010). The Q system: a repressible binary system for transgene expression, lineage tracing, and mosaic analysis. Cell *141*, 536–548.

Preibisch, S., Saalfeld, S., and Tomancak, P. (2009). Globally optimal stitching of tiled 3D microscopic image acquisitions. Bioinformatics *25*, 1463–1465.

Rechsteiner, M., and Rogers, S.W. (1996). PEST sequences and regulation by proteolysis. Trends Biochem. Sci. *21*, 267–271.

Schindelin, J., Arganda-Carreras, I., Frise, E., Kaynig, V., Longair, M., Pietzsch, T., Preibisch, S., Rueden, C., Saalfeld, S., Schmid, B., et al. (2012). Fiji: an open-source platform for biological-image analysis. Nat. Methods *9*, 676–682.

Schmidt, U., Weigert, M., Broaddus, C., and Myers, G. (2018). Cell detection with star-convex polygons. Lect. Notes Comput. Sci. (Including Subser. Lect. Notes Artif. Intell. Lect. Notes Bioinformatics) *11071*, 265–273.

Simon, F., Fichelson, P., Gho, M., and Audibert, A. (2009). Notch and Prospero repress proliferation following cyclin E overexpression in the *Drosophila* bristle lineage. PLoS Genet *5*, e1000594.

Stapornwongkul, K.S., de Gennes, M., Cocconi, L., Salbreux, G., and Vincent, J.P. (2020). Patterning and growth control in vivo by an engineered GFP gradient. Science *370*, 321–327.

Thummel, C.S., and Pirrotta, V. (1992). Technical notes: new pCasper P-element vectors. D. I. S. *71*, 150.

Please cite this article in press as: di Pietro et al., Rapid and robust optogenetic control of gene expression in *Drosophila*, Developmental Cell (2021), https://doi.org/10.1016/j.devcel.2021.11.016



Toettcher, J.E., Voigt, C.A., Weiner, O.D., and Lim, W.A. (2011). The promise of optogenetics in cell biology: interrogating molecular circuits in space and time. Nat. Methods *8*, 35–38.

Viswanathan, R., Necakov, A., Trylinski, M., Harish, R.K., Krueger, D., Esposito, E., Schweisguth, F., Neveu, P., and De Renzis, S. (2019). Optogenetic inhibition of Delta reveals digital Notch signalling output during tissue differentiation. EMBO Rep *20*, e47999.

Wang, X., Chen, X., and Yang, Y. (2012). Spatiotemporal control of gene expression by a light-switchable transgene system. Nat. Methods *9*, 266–269.

Wang, Y., Xu, J., Pierson, T., O'Malley, B.W., and Tsai, S.Y. (1997). Positive and negative regulation of gene expression in eukaryotic cells with an inducible transcriptional regulator. Gene Ther *4*, 432–441.

Weigert, M., Schmidt, U., Boothe, T., Müller, A., Dibrov, A., Jain, A., Wilhelm, B., Schmidt, D., Broaddus, C., Culley, S., et al. (2018). Content-aware image restoration: pushing the limits of fluorescence microscopy. Nat. Methods *15*, 1090–1097.

Weinberg, B.H., Cho, J.H., Agarwal, Y., Pham, N.T.H., Caraballo, L.D., Walkosz, M., Ortega, C., Trexler, M., Tague, N., Law, B., et al. (2019). High-performance chemical- and light-inducible recombinases in mammalian cells and mice. Nat. Commun. *10*, 4845.

Xu, T., and Rubin, G.M. (1993). Analysis of genetic mosaics in developing and adult *Drosophila* tissues. Development *117*, 1223–1237.

Yagi, R., Mayer, F., and Basler, K. (2010). Refined LexA transactivators and their use in combination with the *Drosophila* Gal4 system. Proc. Natl. Acad. Sci. U. S. A. *107*, 16166–16171.

Yamada, M., Nagasaki, S.C., Suzuki, Y., Hirano, Y., and Imayoshi, I. (2020). Optimization of light-inducible Gal4/UAS gene expression system in mammalian cells. iScience *23*, 101506.

Zeidler, M.P., Tan, C., Bellaiche, Y., Cherry, S., Häder, S., Gayko, U., and Perrimon, N. (2004). Temperature-sensitive control of protein activity by conditionally splicing inteins. Nat. Biotechnol. *22*, 871–876.

Zirin, J., Hu, Y., Liu, L., Yang-Zhou, D., Colbeth, R., Yan, D., Ewen-Campen, B., Tao, R., Vogt, E., VanNest, S., et al. (2020). Large-scale transgenic Drosophila resource collections for loss- and gain-of-function studies. Genetics *214*, 755–767.

Please cite this article in press as: di Pietro et al., Rapid and robust optogenetic control of gene expression in *Drosophila*, Developmental Cell (2021), https://doi.org/10.1016/j.devcel.2021.11.016





## STAR★METHODS

### KEY RESOURCES TABLE

| Reagent or resource | Source | Identifier |
|---|---|---|
| Experimental models: Organisms/strains | | |
| Drosophila: Ecad:GFP$^{ki}$ | (Huang et al., 2009); gift of Yang Hong. | NA |
| Drosophila: Ecad:3xmKate2 | (Pinheiro et al., 2017) | NA |
| Drosophila: Ecad:3xTagRFP | (Pinheiro et al., 2017) | NA |
| Drosophila: Ecad:3xiRFP670 | This study. Transgene inserted at the *E-Cad [KO;attP]* attP docking site (Pinheiro et al., 2017). | NA |
| Drosophila: Act5C-Gal4 | Bloomington Drosophila Stock Center. | BDSC#3954 |
| Drosophila: tub-Gal80$^{ts}$ | (McGuire et al., 2001); Bloomington Drosophila Stock Center. | BDSC#7017 |
| Drosophila: Vg-FRT-VgHA-FRT | This study. Transgene inserted at the *vg [KO;attP]* attP docking site (Stapornwongkul et al., 2020). | NA |
| Drosophila: MyoII:GFP$^{ki}$ (Sqh:eGFP) | (Ambrosini et al., 2019); gift of Magali Suzanne. | NA |
| Drosophila: UAS-LifeAct:GFP | Bloomington Drosophila Stock Center. | BDSC#35544 |
| Drosophila: UAS-His2B:RFP | (Langevin et al., 2005) | NA |
| Drosophila: UAS-His2B:YFP | (David et al., 2005) | NA |
| Drosophila: UAS-IVS-CD8:RFP | Bloomington Drosophila Stock Center. | BDSC#32218 |
| Drosophila: UAS-Myr:RFP | Bloomington Drosophila Stock Center. | BDSC#7119 |
| Drosophila: UAS-nls:Scarlet:PEST | This study. Transgene inserted the PBac {yellow[+]-attP-9A}VK00013 attP docking site. | NA |
| Drosophila: UAS-FLP | Bloomington Drosophila Stock Center. | BDSC#8209 |
| Drosophila: UAS-ebony$^{dsRNA}$ | Vienna Drosophila Resource Center. | VDRC#104174 |
| Drosophila: UAS-Dpp | (Dejima et al., 2011) | NA |
| Drosophila: UAS-Zip$^{DN}$:YFP | (Dawes-Hoang et al., 2005); gift of Dan Kiehart. | NA |
| Drosophila: UAS-Nslmb-vhhGFP4 | (Caussinus et al., 2011), referred to as UAS-deGradFP; Bloomington Drosophila Stock Center. | BDSC#38422 |
| Drosophila: UAS-CycE$^{18}$; UAS-CycE | (Simon et al., 2009); gift from Michel Gho. | NA |
| Drosophila: ubi-FRT-stop-FRT-nls:GFP | (Evans et al., 2009); Bloomington Drosophila Stock Center. | BDSC#28281 |
| Drosophila: UAS-GFP | Bloomington Drosophila Stock Center. | BDSC#6874 |
| Drosophila: pdm2-Gal4 | Bloomington Drosophila Stock Center. | BDSC#49828 |
| Drosophila: nos-Cas9SA | (Poernbacher et al., 2019) | NA |
| Drosophila: ubi-Gal4DBD:2xnMagHigh1 | This study. Transgenes inserted at either the PBac{yellow[+]-attP-9A}VK00027 attP docking site at 89E11 or the P{CaryP} attP14 site at 36A10. | NA |
| Drosophila: ubi-2xpMagHigh1:AD | This study. Transgenes inserted at either the P{CaryP}attP2 docking site at 68A4 or at the P{CaryP}attP33 site at 50B6. | NA |
| Drosophila: wg-Gal4DBD:2xnMagHigh1 | This study. Transgene inserted at the *wg [KO;attP]* attP docking site (Alexandre et al., 2014). | NA |

(*Continued on next page*)

Please cite this article in press as: di Pietro et al., Rapid and robust optogenetic control of gene expression in *Drosophila*, Developmental Cell (2021), https://doi.org/10.1016/j.devcel.2021.11.016



***Continued***

| Reagent or resource | Source | Identifier |
|---|---|---|
| Drosophila: ush-Gal4DBD:2xnMagHigh1 | This study. Gal4DBD:2xnMagHigh1 was inserted upstream of the Ush ATG using CRISPR/cas9 mediated homologous recombination. | NA |
| Drosophila: mirr-Gal4DBD:2xnMagHigh1 | This study. Gal4DBD:2xnMagHigh1 was inserted upstream of the Mirr ATG using CRISPR/cas9 mediated homologous recombination. | NA |
| Drosophila: pdm2-Gal4DBD:2xnMagHigh1 | This study. This driver was generated by gene conversion of the pdm2-Gal4 driver. | NA |
| Drosophila: ubi-2xpMag:AD | This study. Transgene inserted by φC31 mediated transgenesis at the P{CaryP} attP2 docking site at 68A4. | NA |
| Drosophila: ubi-2xpMag$^{Fast1}$:AD | This study. Transgene inserted by φC31 mediated transgenesis at the P{CaryP} attP2 docking site at 68A4. | NA |
| Drosophila: ubi-2xpMag$^{Fast2}$:AD | This study. Transgene inserted by φC31 mediated transgenesis at the P{CaryP} attP2 docking site at 68A4. | NA |
| **Oligonucleotides** | | |
| See Table S1B. | | |
| **Recombinant DNA** | | |
| See also Table S1B | | |
| pUbi-p10-attB | This study | NA |
| pUbi-Gal4DBD:2xnMagHigh1 | This study | NA |
| pUbi-2xpMagHigh1:AD | This study | NA |
| pUbi-2xpMag:AD | This study | NA |
| pUbi-2xpMagFast1:AD | This study | NA |
| pUbi-2xpMagFast2:AD | This study | NA |
| pRIV-Gal4DBD:2xnMagHigh1 | This study | NA |
| pRIV-FRT-VgHA-FRT | This study | NA |
| pHR-Gal4DBD:2xnMagHigh1 | This study | NA |
| pHR-mirr-Gal4DBD:2xnMagHigh1 | This study | NA |
| pHR-ush-Gal4DBD:2xnMagHigh1 | This study | NA |
| pCFD5-mirr | This study | NA |
| pCFD5-ush | This study | NA |
| pTV-Gal4DBD:2xnMagHigh1 | This study | NA |
| pCFD4-GalT | This study | NA |
| pUAS-nls:Scarlet:PEST | This study | NA |
| pEcad:3xiRFP670 | This study | NA |
| **Software and algorithms** | | |
| Fiji | http://fiji.sc | SCR_002285 |
| MetaMorph Microscopy Automation and Image Analysis Software | Molecular devices http://www.moleculardevices.com/Products/Software/Meta-Imaging-Series/MetaMorph.html | SCR_002368 |
| ZEN Digital Imaging for Light Microscopy | Zeiss http://www.zeiss.com/microscopy/en_us/products/microscope-software/zen.html | SCR_013672 |
| Graphpad Prism | Graphpad software http://www.graphpad.com/ | SCR_002798 |

(*Continued on next page*)

Please cite this article in press as: di Pietro et al., Rapid and robust optogenetic control of gene expression in *Drosophila*, Developmental Cell (2021), https://doi.org/10.1016/j.devcel.2021.11.016



*Continued*

| Reagent or resource | Source | Identifier |
|---|---|---|
| Matlab | Mathworks http://www.mathworks.com/products/matlab/ | SCR_001622 |
| Python Programming Language | http://www.python.org/ | SCR_008394 |
| Cell Segmentation, tracking and quantification codes | https://github.com/YBellaicheLab/diPietro_et_al_manuscript | https://doi.org/10.5281/zenodo.5636120 |

## RESOURCE AVAILABILITY

### Lead contact

Further information and requests for resources and reagents should be directed to and will be fulfilled by the lead contact, Yohanns Bellaïche (yohanns.bellaiche@curie.fr).

### Materials availability

Flies and plasmids are available from the lead contact.

### Data and code availability

- No large-scale datasets have been generated in this study. The raw microscopy data that support the findings of this study are available from the lead author upon reasonable request.
- Cell segmentation, tracking, and analysis codes have been deposited at: https://github.com/YBellaicheLab/diPietro_et_al_manuscript (https://doi.org/10.5281/zenodo.5636120) and are publicly available.
- Any additional information required to reanalyze the data shown in this paper is available from the lead contact upon request.

## EXPERIMENTAL MODEL AND SUBJECT DETAILS

### Fly stocks and genetics

*Drosophila melanogaster* flies were grown on standard molasses/cornmeal/yeast food at 25°C or 18°C, and experiments were performed at 25°C unless otherwise specified. *Drosophila melanogaster* stocks used in this study and associated references are listed in the key resources table. Both female and male animals were used in all experiments, except in the experiments shown in (i) Figures 5I and 5K and Figure S5I–S5K for which males were used to ensure that MyoII:GFP located on the X chromosome is the only source of MyoII activity; and (ii) in Figure S3J for which females were used to analyze reporter expression in the gut and the ovaries. The embryo, the larva, the pupa, and the adult stage were used. Stocks carrying both pMagnet and nMagnet transgenes were handled in room light and kept inside cardboard boxes. Experimental crosses were protected from light with aluminum foil. Cross handling, embryo/larva/pupa selection and mounting for live imaging were performed in a dark room under amber light (white light lamp source equipped with a 630/692 nm BrightLine® single-band bandpass filter or using three layers of Deep Straw colour filter LP015 (HT-range, Chris James Lighting Filters) over a white light source. Note that classical genetic markers except the orange/red eye colors can be easily identified under amber light illumination. Experiments using the Gal4/UAS and the Gal4/Gal80$^{ts}$/UAS systems (Brand and Perrimon, 1993; McGuire et al., 2003) were performed as previously described (Bosveld et al., 2012).

## METHOD DETAILS

### Molecular biology and transgenesis

Table S1B lists plasmids generated in this study, their parental plasmids and associated references as well as the sequences of the oligonucleotides used to clone them. Synthesized DNA fragments were obtained from IDT (sequences available upon request) and oligonucleotides from Sigma. Cloning was performed by SLIC (Li and Elledge, 2012), Gibson assembly (Gibson et al., 2009) or regular enzymatic digestion and ligation. All DNA constructs were checked by sequencing and full plasmid sequences or maps are available upon request. Transgenesis was performed by either BestGene or the Crick fly facility. The following plasmids and their corresponding transgenes when relevant were generated as follows:

#### *pUbi-p10-attB*

To generate the pUbi-p10-attB vector, a pUbi-SV40-attB vector was first built by amplifying the ubi-p63E promoter sequence and inserting it into the pCasper-hs vector (Thummel and Pirrotta, 1992) using XhoI and XbaI restriction sites to replace the hs promoter, giving rise to the pUbi-p63E-Casper vector. Then, a fragment containing the SV40 3′UTR and an attB site was amplified from the pUAST-attB vector (Bischof et al., 2007) and inserted into the pUbi-p63E-Casper vector using the BglII restriction site to generate the pUbi-SV40-attB vector. The pUbi-p10-attB was then cloned as follows: the endogenous ATG sequence located upstream of the multiple cloning site in the pCasperUbi-SV40-attB vector was removed by PCR amplifying a fragment from the

Please cite this article in press as: di Pietro et al., Rapid and robust optogenetic control of gene expression in *Drosophila*, Developmental Cell (2021), https://doi.org/10.1016/j.devcel.2021.11.016



pCasperUbi-SV40-attB vector itself while excluding the ATG. This PCR fragment was inserted into the pCasperUbi-SV40-attB vector using the XhoI and NotI restriction sites. The SV40 3′UTR was then replaced by a p10 3′UTR amplified by PCR from the pJFRC81-10XUAS-IVS-Syn21-GFP-p10 (Addgene #36432). The PCR fragment was inserted in the modified pCasperUbi-SV40-attB vector using the XbaI and BamHI restriction sites.

***pUbi-Gal4DBD:2xnMagHigh1 and pUbi-2xpMagHigh1:AD***

The pUbi-Gal4DBD:2xnMagHigh1 vector was generated by cloning a Gal4DBD:2xnMagHigh1 synthetic fragment at the Xba1 site of the pUbi-p10-attB vector. The resulting construct was inserted in the fly genome at the PBac{yellow[+]-attP-9A} VK00027 and P{CaryP}attP14 attP docking sites by φC31 site-directed integration (Groth et al., 2004). The pUbi-2xpMagHigh1:AD plasmid was produced by cloning the pMagHigh1-Linker and the Linker-pMagHigh1:AD synthetic DNA fragments at the XbaI site of the pUbi-p10-attB vector. Transgenesis was then performed by φC31 site-directed integration at the P{CaryP}attP2 and P{CaryP}attP33 sites. Subsequently, recombinant lines of ubi-Gal4DBD:2xnMagHigh1 and ubi-2xpMagHigh1:AD on the second and third chromosomes were generated. All data reported in this manuscript were obtained with the ubi-Gal4DBD:2xnMagHigh1 and ubi-2xpMagHigh1:AD recombinant on the third chromosome. Note that the use of a p10 3′UTR terminator in ubi-2xpMagHigh1:AD vector outperforms an hsp27 3′UTR to achieve strong and homogeneous reporter expression.

*pUbi-2xpMag:AD*, *pUbi-2xpMagFast1:AD* and *pUbi2xpMagFast2:AD*: These vectors were generated by cloning at the SpeI site of the pUbi-p10-attB vector, the 2xpMag:AD, 2xpMagFast1:AD or 2xpMagFast2:AD synthetic DNA fragments, respectively. Each transgene was inserted at the P{CaryP}attP2 site by φC31 site-directed integration. The ubi-Gal4$^{MagFast2}$ driver did not induce detectable LifeAct:GFP expression.

***pRIV-Gal4DBD:2xnMagHigh1***

The pRIV-Gal4DBD:2xnMagHigh1 was generated by inserting a NotI-SpeI fragment coming from pUbi-Gal4DBD:2xnMagHigh1 into the original RIV-CHERRY vector (Baena-Lopez et al., 2013). It was subsequently inserted in *wg[KO;attP]* flies (Alexandre et al., 2014) using φC31 site-directed integration to generate the wg-Gal4DBD:2xnMagHigh1 transgenic flies.

***pRIV-FRT-VgHA-FRT***

To generate the RIV-FRT-VgHA-FRT vector, a C-terminal HA tagged version of *vg* was inserted between the FRT sites in the original RIV-FRT-MCS1-FRT vector (Baena-Lopez et al., 2013). This construct was subsequently integrated in the *vg[KO;attP]* stock (Stapornwongkul et al., 2020) using φC31.

*pHR-Gal4DBD:2xnMagHigh1*, *pHR-mirr-Gal4DBD:2xnMagHigh1, pHR-ush-Gal4DBD:2xnMagHigh1, pCFD5-mirr* and *pCFD5-ush*: To insert a Gal4DBD:2xnMagHigh1-p10 3′UTR sequence downstream of a given promoter by CRISPR/Cas9 mediated homologous recombination, we generated a generic vector pHR-Gal4DBD:2xnMagHigh1 composed of an N-terminal Gal4DBD:2xnMagHigh1-p10 3′UTR and a hs-mini-white cassette flanked by two loxP sites (Huang et al., 2009; Pinheiro et al., 2017). To obtain this vector, the mKate2 sequence of the pHR-mKate2 vector (Pinheiro et al., 2017) was replaced by a ISV-Syn21 sequence (He et al., 2019) followed by the Gal4DBD:2xnMagHigh1-p10 3′UTR sequence by cloning them at the BsaI and BamHI sites using SLIC. The pHR-mirr-Gal4DBD:2xnMagHigh1 and pHR-ush-Gal4DBD:2xnMagHigh1 vectors were then generated by inserting a 5′ homology arm at the BsaI site and 3′ homology arm at the SapI site of the pHR-Gal4DBD:2xnMagHigh1 vector; these 5′ and 3′ homology arm sequences correspond to the ones needed to target either the *mirr* or *ush* locus. Guide RNAs used to target the 2 loci were cloned in the pCFD5 vector (Port et al., 2014) at the BbsI site.

*pTV-Gal4DBD:2xnMagHigh1 and pCFD4 –Gal4T*: In order to convert the pdm2-Gal4 driver into a ShineGal4 driver by CRISPR/Cas9 mediated homologous recombination, two vectors were generated: (i) the CFD4-GalT that ensures expression of the sgRNA necessary to induce a double-strand break in the genomic Gal4 sequences; (ii) the pTV-Gal4DBD:2xnMagHigh1 as a template for gene conversion. CFD4 –Gal4T was generated by inserting 2 copies of the sgRNA in the pCFD4 vector (Port et al., 2014). The Gal4 PAM target (CGG) is located exactly 7bp after aa147, the last aa of the Gal4DBD. To generate pTV-Gal4DBD:2xnMagHigh1, the attP site from the original TV$_{\Delta attP}$-PAX-Cherry (Poernbacher et al., 2019) was first removed. Using Gibson assembly, Gal4DBD was then inserted (aa1-aa147) fused to 2xnMagHigh1 and followed by the p10 3′UTR in the 5′MCS. Subsequently, a PCR fragment (1290bp) encoding 430aa of Gal4 ORF (aa148-aa578) was cloned in the 3′MCS using SpeI and ZraI. During homologous recombination, the sequences encoding the Gal4DBD and the Gal4 aa148-aa578 can therefore be used as the 5′ and 3′ homology arms, respectively (Figure S4C). To promote the homologous recombination event, the Gal4 CRISPR target was also introduced upstream the 5′ homology arm, ensuring the linearization of the pTV-Gal4DBD:2xnMagHigh1 upon injection. Importantly, pCFD4-GalT and pTV-Gal4DBD:2xnMagHigh1 can be used to convert any Gal4 drivers into GAL4DBD:2xnMagHigh1 split drivers necessary to generate the corresponding ShineGal4 driver. For conversion of Gal4 to GAL4DBD:2xnMagHigh1, about 200 nos-Cas9 virgins were crossed with 100 males from the pdm2-Gal4 strain. After 3-4 days, around 300-400 embryos were co-injected with a mix of pCFD4-Gal4T (300ng/μl) and pTV-Gal4DBD:2xnMagHigh1 (500ng/μl), prior to germline pole cell formation. Potential insertions were selected based on the 3pax3-CHE fluorescent marker. Five putative candidate pdm2-Gal4$^{MagHigh}$ lines were confirmed by crossing them to a ubi-2xpMagHigh1:AD; UAS-GFP line to analyze GFP expression in the dark and upon illumination.

***UAS-nls:Scarlet:PEST***

The nls and PEST sequences were added to primers used to amplify the mScarlet sequence from the plasmid pmScarlet-H_C1 (Addgene #85043) and the resultant fragment was subcloned as a KpnI-XbaI fragment into the pJFRC81-10XUAS-IVS-Syn21-GFP-p10 plasmid (Addgene #36432). The resulting plasmid, pJFRC81-mScarlet-PEST, was integrated at the PBac{yellow[+]} attP-9A, VK00013 site in the *Drosophila* genome.

Please cite this article in press as: di Pietro et al., Rapid and robust optogenetic control of gene expression in *Drosophila*, Developmental Cell (2021), https://doi.org/10.1016/j.devcel.2021.11.016



#### *pEcad:3xiRFP670*

Three iRFP670 fragments were amplified from the pmiRFP670-N1 vector (Addgene #79987) and cloned as a triple repeated sequence separated by flexible linkers at the NheI site of the pGE-attB-Shg vector (Huang et al., 2009). The resulting plasmid was then inserted at the *Ecad[KO;attP]* site (Pinheiro et al., 2017) using φC31 mediated recombination.

### Animal mounting for imaging

Embryos, larvae and pupae were collected and mounted for imaging in a dark room under amber light.

#### *Embryo*

Embryos prior to cellularization or at around stage 13 were collected, washed in 1X Phosphate-Buffered Saline (PBS) and dechorionated with household bleach for 1-2min. After 3 washes in PBS, embryos were placed on a MatTek dish (MatTek Life Sciences) and covered with PBS for live imaging.

#### *Larva*

For two photon activation experiments, we adapted the method described in (Kakanj et al., 2020) to anesthetize and mount living larvae for tissues imaging in order to perform small-scale experiments and increase viability at pupal stage. Briefly, using a red light in a dark room, 7 to 8 third instar larvae were collected with a soft brush, and placed in small homemade plastic cages allowing vapor exchange (see Figure 4 (Kakanj et al., 2020)). Larvae were then exposed to diethyl-ether vapor for 3min in these plastic cages. Next, larvae were separated and placed on 35mm glass bottom dishes (20mm microwell, MatTek Life Sciences). Larvae were oriented A-P and dorsolaterally with an angle of approximately 45° to expose one of the wing imaginal discs to the glass bottom surface, in preparation for inverted microscopy. After imaging and two-photon photoactivation, larvae were collected and kept in a food vial in the dark, until observation. This protocol allowed us to anesthetize larvae for 30min and to obtain high animal viability after anesthetization (70–100% in more than 10 experiments). To image the UAS-His2B:RFP signal 7h after activation in whole larvae, the above procedure was repeated for anesthetization and observation.

#### *Pupa*

Pupae were collected and mounted for dorsal thorax, wing or histoblast live imaging as described previously (Bosveld et al., 2012; Classen et al., 2008; Pinheiro et al., 2017).

### Larva and adult tissue dissection and staining

#### *Larva*

Third instar wandering larvae were collected and head complexes were dissected in PBS and fixed for 30min in 4% PFA (Electron Microscopy Sciences). Upon 3 washes in PBT (PBS, 0.1% Triton X100, Sigma), head complexes were counterstained with DAPI (4′,6-diamidino-2-phenylindole, 1μg/ml) before dissection of the imaginal discs and the CNS. The imaginal discs and the CNS were either equilibrated in PBS:glycerol (1:1) before mounting them in PBS:glycerol (1:4) with 4% n-propyl gallate, or directly mounted in Mowiol.

#### *Adult*

Adult guts, ovaries and Malpighian tubes were dissected in PBS from fed female flies, and fixed in 4% PFA in PBS for 90min. Upon 3 washes in PBT, they were equilibrated in PBS:glycerol, washed in PBT and then counterstained with DAPI (1mg/ml) in PBT before further dissection, equilibration in PBS:glycerol (1:1) and mounting in PBS:glycerol (1:1) supplemented with 4% n-propyl gallate. To image adult flies in the ebony experiment, animals were immersed in a glycerol:ethanol (4:1) solution to avoid reflection and imaged using a Zeiss binocular equipped with an Axiocam camera and three white light sources (Zeiss KL200LED and Schott KL1600). To image adult flies in the vg experiment, animals were anchored in low-melting agarose and imaged on a Zeiss SteREO Discovery V20 with an Axiocam 105 color camera and built-in white light source. For adult wing imaging, flies were preserved and their wings dissected in 100% isopropanol. Wings were mounted on Euparal mounting medium (Anglian Lepidopterist Supplies, ALS).

### Microscopy and photoactivation

#### *Microscopes, software, and imaging*

Samples were imaged at 25°C, unless otherwise specified, using the following setups: 1) An inverted confocal spinning disk microscope CSU-W1 (Andor/Roper/Nikon) equipped with a sCMOS camera (Flash4 Hamamatsu), and a Borealis module from Andor for better field homogeneity. Pupae were imaged with a 40x objective (NA 1.3 OIL DIC H/N2 PL Fluor). This microscope was used for all time-lapse acquisitions of the pupal notum and single photon photoactivation at 491 nm; 2) An inverted confocal spinning disk microscope from Zeiss (CSUW1, Roper/Zeiss) equipped with a sCMOS camera (Flash4 Hamamatsu), a Visitron module for better field homogeneity and a FRAP module (iLAS) using either 40x NA 1.4 OIL DIC N2 PL FLUOR, a 100x NA 1.4 OIL DIC N2 PL APO VC or 10x NA 0.3 DIC L/N1 PL FLUOR objectives. This set-up was used for the FRAP experiments and acquisition of several still images; for these two microscopes images were taken using a 2x2 binning unless otherwise specified; 3) An inverted confocal microscope from Carl Zeiss (LSM880 NLO) with 40x NA 1.3 OIL DICII PL APO (UV) VIS-IR or with a 25x NA 0.8 OIL, W, Gly LD LCI PL APO (UV) VIS-IR objectives. This microscope was used for still image acquisition, and for local photoactivation (see two photon section) since it is equipped with a two-photon Ti:Sapphire laser (Mai Tai DeepSee, Spectra Physics); a same model microscope with a C-Apochromat 40x NA 1.2 water-immersion objective was used to image wing discs for the pdm2 experiment; 4) An inverted Nikon CSU-W1 Spinning disk microscope equipped with a Prime 95B sCMOS camera (Teledyne Photometrics) and a 40x NA 1.15 Apo LWD Lambda

Please cite this article in press as: di Pietro et al., Rapid and robust optogenetic control of gene expression in *Drosophila*, Developmental Cell (2021), https://doi.org/10.1016/j.devcel.2021.11.016



WI objective. This set-up was used for pupal wing and embryo photoactivation and imaging; 5) A LSM780 NLO inverted confocal microscope (Carl Zeiss) equipped with a Chameleon NIR tuneable two-photon laser (Coherent) and using a 40x NA 1.2 C-Apochromat WI objective. This set-up was used for local photoactivation in pupal wings; 6) A Zeiss Axioplan 2 upright light microscope (Carl Zeiss) equipped with an Axiocam camera, with a 5x dry objective was used to image adult wings. Software packages from Zen, iLAS and Metamorph were used for microscopy.

The image acquisition and photoactivation routines used for each experiment are described in Table S1A. The Metamorph autofocus function was used for all time-lapse acquisitions in the notum. To photoactivate ShineGal4, one should simply first try laser powers routinely used for live imaging in conditions without bleaching and detrimental developmental effects. In the following sections we provide additional details and considerations. We noticed that the fluorescence lamp source (HXP 120V from Zeiss) with a HE DsRed filter (excitation 545/525, dichroic mirror 570) used to observe pupae at 40x prior to imaging/photoactivation can promote the activation of ShineGal4 drivers. We thus recommend using laser illumination to observe and focus samples prior to imaging.

#### *Measurements of laser power*

Single photon lasers: Laser powers were measured on the front focal plane of the objective using a compact power and energy meter console (ThorLabs, #PM100D) fitted with a low power photodiode sensor (ThorLabs, #S170C). Infrared multiphoton laser: Laser power on the focal plane was determined either by i) measuring the power at the back focal plane of the objective with a thermopile sensor (PM10V1, Coherent, Santa Clara, USA) and multiplying by a factor of 0.75 (transmission of the 40x oil objective at 920 nm according to Zeiss transmission curves https://www.micro-shop.zeiss.com/) for the two-photon Ti:Sapphire laser used in most experiments, or ii) on the sample plane (spot scan mode), using a compact power and energy meter console (ThorLabs, #PM100D) fitted with a high power thermal sensor (ThorLabs, #S470C), for the Chameleon NIR tuneable two-photon laser used for local photoactivation in the wing.

#### *Single photon photoactivation using spinning disk microscope*

When using the ubi-Gal4$^{MagHigh}$ or ubi-Gal4$^{Mag}$ drivers, one pulse of 10, 50, 100, or 200ms at 0.5mW 491 nm is sufficient to promote local UAS expression. The reporter expression can also be observed in the tissues beneath the notum. Hence, two-photon photoactivation should be favored to exclusively activate expression in a ROI. Furthermore, several 491-nm illumination pulses leads to photoactivation of all tissues of (i) the pupa under observation and (ii) the other pupae present on the same slide. Thus, non-photoactivated controls are imaged separately. In the case of the ubi-Gal4$^{MagFast1}$ a pulsed illumination (4s pulse, in a 20 z-section x 200 ms/z, every minute for 25min) with 491nm laser (0.5mW) is necessary for reporter expression, which is in agreement with the lower heterodimerization strength reported for the High-Fast1 Magnet pair (Kawano et al., 2015).

#### *Two photon photoactivation*

Two photon based photoactivation was performed with either (i) a Ti:Sapphire laser (Mai Tai DeepSee, Spectra Physics) at 920 nm, using a 40x objective NA1.3 OIL DICII PL APO (optical zoom 0.6x), or (ii) A LSM780 NLO inverted confocal microscope (Carl Zeiss) equipped with a Chameleon NIR tuneable two-photon laser (Coherent) and using a 40x NA1.2 C-Apochromat WI objective.

(i) Pupal tissue photoactivation:

For photoactivation, Ecad:3xmKate2 or Ecad:3xTagRFP were used to visualize tissues and define one or several ROI using Zen Zeiss software. Each ROI was then consecutively scanned (4 iterations per line, pixel dwell time: 0.76μs) several times for an equal number of times at a subapical position (2μm below the apical surface) and at a more basal position, roughly corresponding to nuclei position (4μm below the apical surface). Different laser powers or different total number of scans were used (Table S1A). A slight bleaching of the Ecad:3xmKate signal was sometimes observed when performing the two photon photoactivation routines.

(ii) Imaginal disc photoactivation:

We found that wing discs are located at approximately 30-80μm below the larva epidermis (the first wing imaginal disc nuclei being approximately 40μm below the larval epidermis). To photoactivate them, laser power was set between 108 and 281mW. Note that above 187mW tissue damage starts to be observed in some animals indicated by disorganization of the tissue and the presence of wounds. As the wing imaginal disc is a pseudostratified not flat epithelial tissue, performing two photon illuminations at different z positions improved the efficiency of activation in the designed ROI.

### Photoactivation in whole animals

#### *LED illumination*

Pupae staged between 13 and 20hAPF were placed in a Petri dish (ThermoFisher) with their ventral side facing down. The dish was placed upside down inside a BlueCell device equipped with an array of 460 nm LED strips controlled by a Raspberry Pi microcomputer unit (Gehrig et al., 2017). Similarly, 3$^{rd}$ instar larvae were illuminated using the BlueCell device to induce gene expression in the imaginal discs in the experiment using the pdm2-Gal4$^{MagHigh}$ driver (Figure 4D; Figure S4E).

#### *Ambient light or fiber optic light source*

To induce gene expression from the 3$^{rd}$ instar larval stage onwards using the ubi-Gal4$^{MagHigh}$ driver, larvae were transferred to two new food vials under amber light: one vial was then kept in the dark using an aluminum wrapping, while the other was simply placed on a lab desk at ambient light until fly hatching. A similar protocol was used to expose animals to light throughout their development. Ambient light or Zeiss KL200 LED light source (15mW/cm$^2$) were also used to photoactivate ubi-Gal4$^{MagHigh}$ to induce reporter

Please cite this article in press as: di Pietro et al., Rapid and robust optogenetic control of gene expression in *Drosophila*, Developmental Cell (2021), https://doi.org/10.1016/j.devcel.2021.11.016



expression in 3rd instar larvae and adult tissues by exposing whole animals in vials. For the Figure S1B, a Schott KL 1600 LED white light source with or without amber light filter (630/692 nm BrightLine® single-band bandpass) was used. For the Figure S3H, a transmitted white light Leica stereoscope with or without three layers of Deep Straw colour filter LP015 for amber light was used.

### Figures preparation

Images and time-lapse movies shown as figure panels or time-lapse movies were subjected to bleach correction, brightness, and contrast modifications and rotation using Fiji (Schindelin et al., 2012) or Photoshop. Furthermore, time-lapse movie stacks were registered using the MultistackReg or Linear Stack Registration with SIFT Fiji plugin, to visualize the change in signal level in specific ROI. All images are maximal projections of the relevant z-sections. Full tissues images of the notum, abdomen, wing, wing discs, CNS and embryos were generated by stitching multiple positions using 2D stitching, Pairwise or Grid/Collection, plugins in Fiji (Preibisch et al., 2009). For embryo movies processing, outlier pixels were removed using the Remove Outliers function (radius 2, threshold 10). Then, a radius 1 Gaussian filter was applied, before projection and stitching. For images displayed in Figure 3B and Figures S5J and S5K denoising was performed using the Fiji despeckle filter. In Figures S3G and S3J the DAPI channels were adjusted independently in each image. Graphs were made using GraphPad (Prism) or MATLAB (MathWorks). Error bars are the standard error of the mean (SEM).

## QUANTIFICATION AND STATISTICAL ANALYSIS

### Quantifications

#### *His2B:RFP and nls:Scarlet:PEST signals*

The UAS-His2B:RFP or UAS-nls:Scarlet:PEST signals were quantified as their mean intensity on maximal projections within a given ROI either on one image or on the successive time-lapse images using a Fiji macro. Mean background intensities were determined as the mean value either measured at the beginning of the experiment for time-lapse movies or measured outside the tissue in the case where the total RFP signal was integrated over the whole tissue. In experiments for which Ecad:3xmKate2 was used to label the tissue, the mean RFP signal was corrected by subtracting the mean RFP signal measured in pupae of the same genotype and at the same time-points without photoactivation. This ensures that the Ecad: 3xmKate2 signal is not taken into consideration when measuring the RFP signal. All mean corrected values were normalized to the maximal value in time-lapse experiments. For the FRAP experiments, the UAS-His2B:RFP mean intensities measured within the photobleached area over time were normalized by one of a neighboring non-bleached area over time. The switch-on $t_{1/2}$ was determined on individual His2B:RFP, His2B:YFP and LifeAct:GFP level curves and individual values were then averaged. To determine when the His2B:RFP or nls:Scarlet:PEST signals start to decrease upon reaching their maxima, we quantified the time at which the fluorescent level decreases by 10% relative to its maximal level on each curve. These values were then averaged.

#### *Cell division rate*

Upon live-imaging, Ecad:3xmKate2 image stacks were restored and projected using CARE (Weigert et al., 2018). For the few time-points for which the focus was lost, these time-point images were replaced by a previous time point acquisition to facilitate segmentation and tracking. The cell outlines were then segmented using a homemade segmentation software based on watershed and StarDist (Schmidt et al., 2018). Cell tracking was performed and division rates were determined using MATLAB and C++ codes as previously published (Bosveld et al., 2012; Guirao et al., 2015; López-Gay et al., 2020).

#### *Cell apical area*

In the case of the $Zip^{DN}$ and deGradFP/MyoII:GFP experiments, Ecad:3xmKate2 z-stacks were projected using CARE (Weigert et al., 2018). The segmentation was then performed as indicated for the division rate quantification. Each cell area was finally measured using MATLAB codes in both the photoactivated and the corresponding control regions. Microchaetea and macrochaetea were excluded from the analyses.

#### *Vein phenotype*

Classification of the phenotypic severity of ectopic vein phenotypes in adult wings was performed by visual inspection. The criteria used for classification was the extent of ectopic vein coverage. Phenotypes were classified as mild for an ectopic vein coverage of up to 50%, moderate for an ectopic vein coverage of 50–80% and severe when the whole wing was covered by ectopic vein tissue.

### Statistics

Sample sizes vary in each experiment. The experiments were performed on a minimum of 3 animals per condition. Animals were randomly selected within a given genotype for subsequent analyses. Only animals without developmental delay and normal Ecad distributions (when applicable) were included in the analyses. In Figures 5G, 5J, and 5K and Figure S5H: Cells at the border of images were not quantified as they cannot be properly segmented. The adult phenotypes shown in Figures 5A and 5B and Figures S5A and S5B are representative of at least 15 animals. To determine the statistical difference between sets of continuous data, we performed non-parametric Mann-Whitney tests on GraphPad. Significance is indicated by asterisks: *, $p<0.05$; **, $p<0.01$; ***, $p<0.001$; and ****, $p<0.0001$. No blinding was performed. The statistical parameters are reported in figure legends. N indicate the number of animals and the error bars represent the standard error of the mean (SEM).